Pontificia Universidad
JAVERIANA
Cali

Electrochemical Non-invasive Biosensors for Humans and Plants Health Monitoring

Dissertation submitted in partial compliance of requirements for the degree of Doctor of Engineering and Applied Sciences at the Pontificia Universidad Javeriana in Cali

by

Sammy A. Perdomo

PhD Advisor:

Prof. Andres Jaramillo-Botero, PhD.

2023

Dedication

In the loving memory of my beloved grandparents who guided me along life's arduous path and gave me their boundless love. To my loving wife, whose endless love and unwavering support have been instrumental in shaping our shared future. To my dear friends and all the people who have extended their helping hand, I will be eternally grateful for their presence on my journey.

Epigraph

“The simple things are also the most extraordinary things, and only the wise can see them.”

— Paulo Coelho, The Alchemist

Table of Contents

List of Figures

List of Tables

Abbreviations

POC	Point-of-Care
SPCE	Screen-printed Carbon Electrode
LIG	Laser-induced Graphene
LOD	Limit of Detection
LOQ	Limit of Quantification
RT-PCR	Reverse Transcription Polymerase Chain Reaction
SA	Salicylic Acid
ISE	Ion Selective Electrodes
ISM	Ion Selective Membrane
AA	Ascorbic Acid
EDL	Electrical Double Layer
GCE	Glassy Carbon Electrodes
CVD	Chemical Vapor Deposition
BDD	Boron Doped Diamond
mAbs	Monoclonal Antibodies
SNR	Signal-to-Noise Ratio
FET	Field-effect Transistor
ADC	Analog to Digital Converter
DAC	Digital to Analog Converter
OCP	Open Circuit Potential
WE	Working Electrode
RE	Reference Electrode
CE	Counter Electrode
TIA	Transimpedance Amplifier
PCB	Printed Circuit Board
CV	Cyclic Voltammetry
DPV	Differential Pulse Voltammetry
CA	Chronoamperometry
LSV	Linear Sweep Voltammetry
EIS	Electrochemical Impedance Spectroscopy
PET	Polyethylene Terephthalate
PBS	Phosphate Buffer Solution
PI	Polyimide
PVA	Polyvinyl Alcohol
RMS	Root Mean Square
GUI	Graphical User Interface
RI	Reverse Iontophoresis
BSA	Bovine Serum Albumin

Acknowledgements

First, I would like to thank my PhD advisor professor Andres Jaramillo-Botero, for his exceptional guidance through this amazing journey. His great experience, knowledge, intensive work, and the trust that he put on me give me the opportunity to accomplish more than I ever would have expected. Working with him has shown me the importance of the interdisciplinary education for my professional development and the infinite possibilities that we, as scientists, have to offer for the development of our loved country.

Also, I would like to thank to Prof. Drochss Pettry Valencia, for his support, knowledge and dedicated teamwork that made possible the success of our joint projects. Additionally, I offer special thanks to Prof. Mauricio Quimbaya for all the knowledge that he shared with me. My heartfelt appreciation also goes out to all the members and co-workers of the Omicas Institute for their contributions to my research.

During my PhD internship, I had the privilege of working with Professor Joseph Wang and his Nano bioengineering research team at UC San Diego. I would like to express my sincere gratitude to Professor Wang, Ernesto de la Paz, Rafael del Caño, Sumeyye Sekker, and Tamoghna Sano for their knowledge, experience, collaboration, and significant contributions to this dissertation. I especially value the friendship and admirable support provided by Ernesto de la Paz and Rafael del Caño.

I would also like to acknowledge the tremendous support provided by my dear friends Eduardo Marin, Jingcheng Ma, and Alberto Gonzalez. Their significant presence, encouragement, and willingness to lend a helping hand during challenging times have been instrumental in keeping me motivated and focused.

Last but not least, I am deeply grateful for the scholarship provided by the Omicas Alliance (Optimizacion Multiescala In-silico de Cultivos Agriculas Sostenibles: Infraestructura y validación en Arroz y Caña de Azúcar). This scholarship has been instrumental in funding my PhD journey and facilitating my academic and research development.

Publications

This PhD dissertation is based on the work contained in the following papers:

I. Perdomo, S. A., Marmolejo-Tejada, J. M., & Jaramillo-Botero, A. (2021). *Bio-nanosensors: Fundamentals and recent applications*. Journal of The Electrochemical Society, 168(10), 107506. DOI: 10.1149/1945-7111/ac2972

II. Perdomo, S. A., Ortega, V., Jaramillo-Botero, A., Mancilla, N., Mosquera-DeLaCruz, J. H., Valencia, D. P., et al. (2021). *SenSARS: A low-cost portable electrochemical system for ultra-sensitive, near real-time, diagnostics of SARS-CoV-2 infections*. IEEE Transactions on Instrumentation and Measurement, 70, 1-10. DOI: 10.1109/TIM.2021.3119147

III. Perdomo, S. A., De la Paz, E., Del Caño, R., Seker, S., Saha, T., Wang, J., & Jaramillo-Botero, A. (2023). *Non-invasive in-vivo glucose-based stress monitoring in plants*. Biosensors and Bioelectronics, 231, 115300. DOI: 10.1016/j.bios.2023.115300

IV. Perdomo, S. A., Valencia, D. P., and Jaramillo-Botero, A. *Wearable Electrochemical Biosensor for Non-destructive, In-situ, In-vivo, and Real-time Salicylic Acid Detection in Plants: Advancing Abiotic Stress Monitoring*. (In preparation for submission, 2023).

Abstract

Non-invasive biosensors offer significant advantages over traditional invasive methods, as they eliminate discomfort, reduce risks of infection, and enable continuous monitoring without disruption. In humans, these sensors enable the possibility of early disease diagnostic even before symptoms manifest, leading to improved disease management and more effective treatment strategies. In the agriculture field, non-invasive biosensors offer a non-destructive and efficient approach to assess plant responses to environmental stresses. By understanding how plants adapt and respond to different biotic and abiotic stresses, researchers can develop strategies for crop improvement, optimize resource utilization, and enhance agricultural productivity in a sustainable manner. However, there are several challenges that need to be addressed, which include improving the sensitivity, selectivity, and stability of the biosensors, as well as enhancing their compatibility with diverse plant species and environmental conditions. Additionally, novel strategies are needed to expand the range of analytes that can be detected non-invasively, allowing for a comprehensive understanding of plant physiological processes. Research on novel non-invasive biosensors holds immense potential for advancing healthcare practices, promoting preventive medicine, and enhancing our understanding of plant stress physiology, thereby contributing to human well-being and global food security.

This dissertation presents the development and application of three novel biosensor platforms for non-invasive health monitoring in both humans and plants. The first platform is based on a stand-alone point-of-care (POC) device for rapid (< 10 min) SARS-CoV-2 diagnosis infection in human swab or saliva using an antigen modified screen-printed carbon electrode (SPCE) and electrochemical impedance spectroscopy (EIS) technique as quantification method. The sensor exhibits an impressive limit of detection (LOD) of 1 fg/mL and a remarkable selectivity (> 90%). These achievements represent substantial enhancements, with the LOD surpassing traditional RT-PCR methods by over 23% and an astounding 99.98% improvement compared to a relevant vertical-flow cellulose-based technology currently available. Additionally, this innovative technology reduces the diagnostic time to just 10 minutes, marking a remarkable 91.67% improvement compared to the time-consuming RT-PCR method and an important 33.33% reduction compared to similar approaches. In the second platform, a chronopotentiometry wearable biosensor, based on an iontophoretic system for plant exudation and a glucose oxidase (GOx) modified SPCE, is proposed for glucose determination in plants under light and temperature stress. This sensor achieves a low LOD of 9.4 µmol L^{-1} and demonstrates a

sensitivity of 22.7 nA/µmol L^{-1}·cm^{-2}, exposing significant improvements of over 130.98% and 99.95%, respectively, compared to a relevant microneedle-based biosensor designed for *in-vivo* glucose monitoring in plants previously published in the state of the art. In the last platform, a bioagent-free chronopotentiometry wearable biosensor based on the iontophoretic system and a laser-induced graphene (LIG) electrode is proposed for non-invasive salicylic acid monitoring in plants under drought and salinity stress. With a sensitivity of 82.3 nA/µmol L^{-1}·cm^{-2} and an LOD of 8.2 µmol L^{-1}, the proposed sensor demonstrates remarkable improvements of over 99% in sensitivity and 90% in linearity, compared to the first non-invasive SA biosensor presented in the state of the art. Overall, the presented platforms represent significant advancements in the field. These biosensors hold great potential for revolutionizing healthcare and agriculture, enabling efficient and timely monitoring of health conditions, stress responses, and disease detection.

Keywords: Non-Invasive biosensors, electrochemical impedance spectroscopy (EIS), chronoamperometry, chronopotentiometry, SARS-CoV-2, abiotic plant stress monitoring.

Introduction

In recent years, biosensors have emerged as powerful tools for detecting and quantifying biological analytes in various fields, including human healthcare and agriculture[1,2]. A biosensor integrates a biological recognition element, such as enzymes, antibodies, or nucleic acids, with a transducer (electrode) to convert the biological or chemical response into a measurable signal[3]. The development of biosensors has opened new avenues for non-invasive sensing technologies, offering advantages over traditional invasive methods such as lower fabrication costs, ultrahigh sensitivity and selectivity, real-time response, and the elimination of invasive procedures like blood sampling or tissue biopsies[4].

In the human healthcare field, there has been increasing attention on the development of novel non-invasive sensors that combine the portability of wearable devices with the efficient detection of ultra-low concentrations of analytes of interest[5–8]. These sensors have extended their use to monitoring disease-related metabolites (glucose[9], lactate[10], ketones[11], etc.) and viruses (influenza[12], SARS-CoV-2[13], HIV[14], Ebola[15], etc.), enabling early disease detection and personalized healthcare. However, wearable biosensors in healthcare face several challenges that need to be addressed for widespread adoption[16]. These challenges include understanding the correlation between analyte concentrations in blood and non-invasive biofluids, developing new bioaffinity assays and sensing strategies, conducting large-scale validation studies, and commercializing reliable and accurate wearable biosensing platforms. Issues such as surface fouling, stability, calibration, and fluid sampling systems must also be addressed. Additionally, the composition of biofluids and their relation to blood chemistry and medical disorders should be better understood. Rigorous interpretation of biosensor data, correlation studies with blood assays, and integration with medical data mining and machine learning are crucial for the successful realization of wearable biosensors in healthcare. Ensuring accuracy and reliability of wearable sensor responses is vital for market acceptance and requires addressing challenges related to surface fouling, biofouling, and stability under uncontrolled conditions.

Similarly, in the agriculture field, innovative biosensors have been proposed to effectively monitor water availability[17–19], soil nutrient levels[20–23], environmental stressors[24–29], disease and pest presence[30–36], pesticides[37–41], and endogenous metabolites[42–55]. These biosensors aim to improve the understanding of plants' biological processes, especially considering the significant impact of climate change on crop productivity worldwide[1,56–58]. Climate change, with its rising temperatures, changing precipitation patterns, and increasing frequency of extreme weather

events, poses a major challenge to agricultural productivity. Abiotic stresses such as drought[59,60], heat[61], cold[62], salinity[63], floodings[64], light[65,66], and heavy metals[67] are exacerbated by climate change, disrupting plant physiological processes, reducing nutrient uptake, impairing photosynthesis, and increasing susceptibility to diseases and pests. Consequently, crop yields are negatively affected, leading to economic losses and food security concerns. Novel biosensor technologies are required to monitor and manage these abiotic stresses by providing real-time, non-invasive measurements of metabolites and enabling early detection of stress conditions for timely interventions[1,68–72]. However, despite the significant progress in the development of these sensing technologies, there are still challenges that need to be addressed to ensure their scalability and global market introduction[73]. Two major challenges include the clean extraction of plant metabolites without affecting the plant and the selective and sensitive detection of target metabolites in complex plant matrices. Interfering substances, such as pigments or secondary metabolites, can impact the accuracy and reliability of biosensor measurements. Additionally, the stability and longevity of biosensors in plant environments, characterized by varying pH, temperature, and humidity, pose challenges for long-term monitoring.

In this dissertation, the focus will be on the fabrication of non-invasive platforms for quantifying metabolites related to human health and plant stress response. To address the pressing need for rapid and accurate detection of SARS-CoV-2, the virus responsible for the COVID-19 pandemic, the first developed platform is an electrochemical POC device that utilizes cutting-edge technologies and methodologies. This device enables rapid (<10 min), sensitive, and specific detection of the virus in human swab or saliva. The sensor has demonstrated remarkable performance, exhibiting high sensitivity and selectivity, thus making it a promising tool for efficient and early diagnosis of SARS-CoV-2 infections. Additionally, to comprehend the impact of abiotic stresses, such as extreme temperatures, light, drought, and salinity, on plant health, two wearable biosensors have been developed as the second and third platforms. These biosensors allow real-time monitoring of glucose and salicylic acid levels. It offers a non-invasive and non-destructive approach by integrating an iontophoretic system, which induces plant exudation. Through this integration, valuable insights into the physiological response of plants to abiotic stresses are obtained, aiding in the implementation of effective stress management strategies. Thereby, these technologies serve as a valuable tool for researchers and farmers, enabling them to monitor metabolite levels in plants and facilitating the early detection of stress and disease conditions. Consequently, timely intervention measures can be undertaken.

Background: Electrochemical Biosensors, Fundamentals and Recent Applications

Electrochemical methods are used to measure the presence of an analyte from the detection of changes in potential, current, resistance or conductivity produced by a chemical redox-type (reduction-oxidation) reaction that takes place inside an electrochemical cell. The analyte of interest is contained in an electrolyte solution that interacts (conventionally) with three electrodes, which act as the sensor's transducer (Figure 1). Two key aspects define the electrochemical biosensor: 1) the working electrode and 2) the electrochemical technique. The working electrode types are primarily categorized as carbon-based electrodes, which include mercury drop electrodes, glassy carbon electrodes, diamond electrodes, carbon paste electrodes, screen-printed electrodes, and paper-based electrodes.

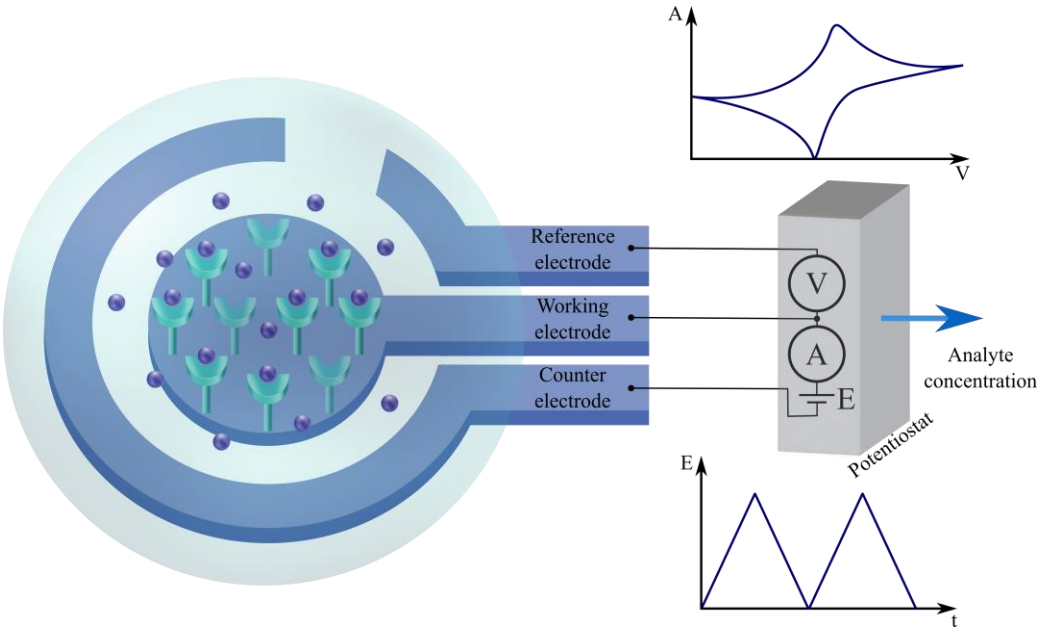

Figure 1. Electrochemical biosensor with three electrodes configuration. Purple-spherical markers represent the target analyte. A redox type reaction occurs on the surface of the working electrode due to the interaction between the functionalized electrode and the target analyte. As result of this chemical process, a current flow through the working and counter electrode. If the analyte is reduced at the working electrode the current is a cathodic current, while the analyte oxidation produces an anodic current. The potentiostat ensures the required voltage conditions on each electrode and measure the faradaic current.

Currently, the most common electrochemical techniques are potentiometric, conductometric, voltammetric, amperometric and impedimetric[74,75]. Recently, unlike these conventional techniques, photoelectrochemical (PEC) biosensing has drawn tremendous attention from researchers in the field of biosensing. PEC sensors are based on a photo-to-electric conversion process, where a photocurrent is obtained under the excitation from an external light source, which improves the sensitivity of the method compared with the traditional techniques[76]. Zeng et al. developed an advanced photoelectrochemical platform for the determination of Kana antibiotic by coupling palindromic molecular beacon based strand-displacement recycling amplification with bismuth oxychloride (BiOCl-Au)-CdS quantum dot (QDs)-based Z-scheme photoinduced reaction system[77]. This sensor used for the first time the palindromic molecular beacon as nucleic acid based amplification technique improving sensitivity and limit of detection (29 fmol L^{-1}).

Traditional electrochemical techniques and electrode types are discussed next.

Electrochemical Techniques

Potentiometric methods are based on the measurement of charge potential at the working electrode. This potential results from the chemical reactions that take place inside the sample solution due to the analyte concentration at the reference electrode, and under condition of non-current flow. The measured potential corresponds to the separation of charge across an interface that directly depends on the electrode type and can be described using the Nernst equation, which allows the calculation of ionic activities or effective concentration as a function of the electrode potential and a standard potential[78]. Lv et al. used a sensor of this type for detection of prostate-specific antigen (PSA) and proposed an *in-situ* signal-amplification strategy to overcome weak electrical readout[79]. This strategy consists of using oligonucleotides and detection antibody-labeled gold nanoparticles as the signal-generation tags on anti-PSA capture antibody-modified glassy carbon electrode with a sandwich-type assay mode. The results indicated an improved performance of the sensor characterized by high sensitivity and a low LOD (13.6 pg mL^{-1}).

There are two types of electrodes commonly used in potentiometric methods: metallic and ion selective electrodes. Metallic electrodes work as a direct indicator of the metal's cation in solution, through a redox reaction that develops an electrical potential depending on the equilibrium between the cation and the electrode surface. Ion selective electrodes (ISE) on the other hand, are capable of selectively measuring the activities of a specific ion using a permeo-selective membrane or ISM and the resulting potential depends on an ion transport process

between an inner membrane solution containing the ion of interest at a fixed activity and the outer solution with the target analyte, resulting in charge separation or a phase-boundary potential across the membrane. The membrane can be composed of silicate glass, inorganic salts, viscous organic liquids or polymers, and must be non-soluble in the analyte solution, electrically conductive and highly selective to the analyte of interest. In practice, the membrane interface is not only permeable to a specific ion, which causes undesired ions to interfere and produce additional charge. In these cases, the Nernst equation can be derived in the Nikolsky-Eisenman equation, which allows the estimation of a sensor's selectivity and LOD[80, 81]. The increasing interest in the use of potentiometric sensors for biological applications has given rise to the development of novel models. For example, a sensitive potentiometric ascorbic acid (AA) biosensor was introduced in[82]. It uses a magnetic beads-ascorbate oxidase/graphene oxide/zinc oxide (MBs-AO/GO/ZnO) membrane-based screen-printed electrode to improve sensitivity, selectivity and LOD for AA, in comparison to other AA sensor models. Recently, Silva et al. reported the use of a paper-based strip electrode in a label-free potentiometric immunosensor for Salmonella typhimurium detection, showing two different immunosensig interfaces assembled on the electrode surface to control an ionic flux through a poly(vinylchloride) carboxylated (PVC–COOH) membrane[83]. Enzymatic biocatalytic precipitation and nanogold labeling techniques have been used to improve the sensitivity in potentiometric immunosensors response[84]. The logarithmic dependence between the chemical potential and the analyte activity, as expressed by the Nernst equation, leads to a low sensitivity in potentiometric ion sensors. To overcome this, a recently coulometric transduction method for solid-contact ion selective electrodes (SCISEs) was introduced, which lowers membrane resistance and improves response time[85].

Voltammetric methods involve a time dependent potential applied to the working electrode. The changing potential leads to a current flow --involving a chemical redox reaction in the sample solution-- between the working and reference electrodes, which provides quantitative and qualitative information associated to the target analyte. Depending on the oxidation or reduction process, the current flows through the working to the counter electrode (also known as a faradaic current). If the analyte is reduced at the working electrode, the faradaic current is a cathodic current, while the analyte oxidation produces an anodic current. The magnitude of this current is determined by the rate of the redox reaction, which is proportional to the rate of the mass transport to and from the electrode and electron kinetics[86]. The mass transport represents the rate at which the involved chemical species move toward or away the electrode surface and can be expressed through diffusion, migration and convection modes. The diffusion mode is based on the movement of ions or molecules, due to the different analyte concentrations on the

electrode surface and the bulk solution. In convection, the motion occurs when the solution is mechanically mixed. During the migration mode, reactant and products move due to the electrode surface charge. Voltammetric processes generally occur in the region where the diffusion is the only significant influencing mode in the mass transport. The rate at which electrons move in the redox process, i.e., electron kinetics, also affects the current. If the electron kinetics are fast, the redox process is reversible and at equilibrium. If the electron kinetics are slow, the redox process is irreversible, and the chemical reaction is not described by the Nernst equation. In addition to the faradaic current, other non-faradaic or background currents exist that can affect the voltammetric measurements. This current is typically related to the redox reaction of impurities, at the bulk solution and the electrode surface charge that leads to the formation of a structured electrode solution interface also known as electrical double layer (EDL).

The different existing voltammetry techniques are uniquely classified based on the applied time-based potential characteristics[87]. The most common techniques include linear sweep and cyclic voltammetry. Each one results in a plot or voltammogram of current vs applied potential, where the current is a function of the target analyte's concentration. In linear sweep voltammetry, a linear potential ramp is applied to scan either oxidation or reduction reaction, whereas in cyclic voltammetry positive and negative potentials are used to scan both analyte oxidation and reduction process. In the cyclic process, the current response has separate current peaks for oxidation and reduction processes. If an irreversible redox reaction takes place just one of these peaks is defined[88].

Aptamer-based voltammetric biosensors have attracted great attention in early disease diagnosis. Linlin Li et al. introduced a novel voltammetric sensor for *Mycobacterium tuberculosis* (MTB) early detection using the ESAT-6 antigen secreted by the bacteria as target analyte, and a glassy carbon electrode (GCE) with reduced graphene oxide with metal-organic framework (MOF-rGO) deposited on the surface[89]. Toluidine Blue (TB) was immobilized on the GCE and platinum/gold core/shell (Pt@ Au) was used to assemble thiolated ESAT-6 binding aptamer on the electrode and further response amplification. The sensor performance exhibited excellent specificity and favorable spike recovery for ESAT-6 detection. For voltammetry immunosensors in health care, a novel signal amplification strategy is introduced in[90]. It is based on two current changes produced by the synergism between the degradation of methylene blue and non-conductive calcium carbonate spheres, which is used for CA199 detection and improves the overall sensor sensitivity. Other fields of application have been successfully demonstrated using voltammetric techniques. For example, in food monitoring applications, the sensitive detection of

heavy metals, such as mercury ions, is important to food safety. In pharmaceutical analysis, voltammetry biosensors performance has been improved by using carbon paste electrodes. For instance, Vieira Thomaz employed a nanostructured TiO_2/carbon graphite matrix in the development of a laccase (Lcc) carbon paste biosensor for paracetamol detection, improving the sensor response with low LOD and good sensitivity[91].

The *Amperometric* technique is similar to the voltammetric one, albeit the applied electrical potential to the working electrode is constant and the current is measured as a function of time compared to the reference electrode. The oxidation or reduction reactions occur at the electrode surface. This method has a higher sensitivity when compared with the potentiometric technique. The amperometric technique is commonly used in biocatalytic and affinity sensors, due to its simplicity and low background current effect[92]. Recently, Cordeiro et al. introduced the use of coated tungsten (W-Au) microelectrodes functionalized with permeo-selective membranes, for biocatalytic sensors[93]. This microelectrode improved the sensitivity and selectivity of glucose monitoring in human brain. Multiplexing to the simultaneous detection of several analytes is an important capability in biomarker sensing. Printed multiplexed amperometric biosensors have been demonstrated on nanostructured conductive hydrogels in[94]. Moreover, Kucherenko et al. presented a biosensor array for the simultaneous determination of glutamate, glucose, choline, acetylcholine, lactate and pyruvate, by immobilizing selective enzymes on the surface of amperometric platinum disc electrodes, demonstrating good selectivity and reproducibility capabilities[95].

In health monitoring, Guerrieri et al. presented a novel highly selective amperometric biosensor for choline determination in patients with renal diseases based on choline oxidase immobilized by co-crosslinking on a Pt electrode with a novel anti-fouling and anti-interferent membrane, that aim to improve the interference rejection, stability and selectivity of the device[96]. In the precision agriculture field, pesticide control is an important topic for environmental safety. Recently, a novel amperometric biosensor was presented by B. Jiang et al. for organophosphorus pesticides determination using an ionic layer-by-layer self-assembly technique, colloidal AuNPs and a p-aminobenzenesulfonic acid-modified glassy carbon electrode with immobilized diazo-resins (DAR) on the surface[97]. This sensor exhibited improved precision, stability and low LOD.

In *conductometry*, changes in conductivity are measured from the analyte or medium involved in chemical reactions. Conductivity is expressed as the ability to conduct a current. If the media is a solution containing ions, its conductivity depends on the ion's mobility between the electrodes, where the bulk solution acts as an electrical conductor. Also, the immobilization of

species on the electrode surface can produce changes in the conductivity of the electrode when detecting binding events with the target analyte. This technique is characterized by its simplicity and the no dependence on a reference electrode, and faradaic effects[98]. Conductometry has been widely used for biosensors in environmental monitoring and clinical analysis applications. A novel conductometric immunosensing platform for highly sensitive detection of prostate cancer marker is developed in[99] by using tetracyanoquinodimethane (TCNQ)-doped thin films of copper-MOF and $Cu_3(BTC)_2$, assembled on gold screen-printed electrodes. Target specific antibodies related to the prostate cancer antigen (PSA) were immobilized on the electrode surface. The doping process improved the overall conductance reaching low LOD and good linearity. In the environmental monitoring field, a recent study by Kolahchi et al. presented a sensitive miniaturized conductimetric biosensor for phenol detection[100]. The sensor was developed by immobilizing *Pseudomonas sp*. (GSN23) bacteria on the surface of gold interdigitated microelectrodes.

Last but not least, the EIS technique is based on a small AC potential signal applied to the working electrode, in order to measure the alternate current resulting from the chemical reaction[101,102]. The impedance response can be analyzed from the relation between the applied voltage and output current and has both magnitude and phase. The applied signal frequency is varied over a wide range for obtaining the impedance spectrum. Then, the equivalent resistance and capacitance can be determined by the in-phase and out-phase current responses, i.e., current can be i) in phase, with the voltage signal in a resistive behavior, and ii) out of phase, if a capacitive behavior is presented. The resistive components include the sample solution resistance, charge transfer resistance and mass transfer resistance. The capacitive components are defined by the electrical double layer (EDL) on the electrode-sample solution interface. The charge and mass transfer resistance are related to the electron kinetics and diffusion mass rate at the chemical redox reaction, respectively.

EIS is capable of sampling electron transfer at high frequency and mass transfer at low frequency[103]. If the overall impedance response of the electrochemical system is determined by the mass transfer behavior, the chemical redox reaction is interpreted as reversible. In contrast, if the electron transfer behavior predominates, the chemical redox reaction is irreversible. The EIS technique is insensitive to environmental disturbance and offers a good signal to noise ratio. Commonly, impedance applications are related to affinity sensors designs[104].

A novel EIS biosensor was developed by Bahner et al. for the detection of doxorubicin, a pervasive cancer treatment drug[105]. The sensor is based on the daunorubicin-binding aptamer,

used as recognition element, and is immobilized with mercaptohexanol on gold. The overall sensor performance is characterized by a linear relationship between the charge transfer resistance and the doxorubicin concentration, resulting in high sensitivity, selectivity and low LOD. In the food monitoring field, Elshafey and Radi presented an EIS biosensor for the determination of alachlor (ALA) in human food[106]. The sensor uses a molecularly imprinted polymer (MIP), immobilized onto a glassy carbon electrode by electrodeposition of o-phenylenediamine (o-PD).

Electrochemical Electrodes

Mercury drop electrodes were widely used in electrochemical techniques such as voltammetry. Mercury electrodes continuously drops into the solution through a capillary tube, thereby constantly renewing the electrode surface, hence guaranteeing reproducible and repeatability current-voltage curves. Unfortunately, this electrode has been restricted for *in-vitro* biological applications due to toxicity considerations[107].

Carbon-based electrodes are established as a good alternative due to their biocompatibility and useful properties, as chemically inertness, reduction of background currents, broad potential windows, optimal surface chemistry and high stability against corrosion[108, 109]. Ryu et al. fabricated a carbon-based electrode by plasma-enhanced chemical vapor deposition (CVD) of vertically aligned nanotubes on a graphite foil substrate, which showed high chemical active area and electrocatalytic affinity for high performance in electrochemical applications[110].

Glassy Carbon electrodes, also known as vitreous carbon electrodes, offer similar properties to the carbon-based electrodes, yet they are impermeable to gases, have extremely low porosity, are compatible with all common solvents, and are not chemically inert under electrochemical oxidation at high anodic potentials[111]. Yi et al. showed that the performance of a glassy carbon electrode under electrochemical oxidative conditions causes morphology changes on the electrode's surface[112].

Diamond electrodes have attracted great attention in recent years for electrochemical sensing applications, given that they can work under extremely high anodic potentials and exhibit robustness to aggressive chemical media in comparison with other electrodes. Furthermore, diamond has unique properties, including a high atomic density, good optical response (i.e. transparency), chemical inertness, and high thermal conductivity, albeit it is an electrical insulator. To improve its electrical conduction, diamond is doped with boron (BDD) showing an extremely high structural stability, while being insensitive to oxygen evolution, enabling low signal to noise

ratios and an enhancement of the potential window[113,114,115]. BDD sensors have been demonstrated in the early detection of influenza[12] and other related applications[116,117,118].

Carbon paste electrodes are the result of combining graphene powder with insoluble organic binders. This type of electrodes exhibit fast surface renewal, low background current, polarizability, modifiable structure and high reproducibility, although the organic solvent can affect the organic binder, decreasing the overall electrode´s performance[119,120].

Screen-printed electrodes are based on the screen-printing technology of graphite powder, or any other ink onto a polymer, ceramic or an inert substrate. This type of electrode is usually designed for single-use, has a small form factor, and provides important analytical features, albeit its kinetics are slow[121, 122, 123, 124].

Paper-based electrodes are composed of cellulose fibers. These exhibit high mechanical flexibility, have reduced thickness and provide a porous open structure capability. Printing techniques allows different materials to be deposited on paper, including carbon nanomaterials, with improved electronic transport response[125]. Preston et al. reported a novel silver nanowire (Ag NW) paper hybrid electrode with stable optoelectronic properties, high transmittance and low sheet resistance due to its grater optical haze[126].

Each one of the above electrodes can be used in any electrochemical technique. Generally, the choice depends on the analyte of interest, its chemical properties, and the sensing requirements. The most used electrochemical sensors are three-electrode systems: with working, reference and counter electrodes. The working electrode handles the chemical reactions of the target analyte, the reference electrode provides a stable (unchanging) potential during the reaction processes at the working electrode (typically based on a conductive material or semiconductive polymer). The faradaic currents from chemical reactions flows through the working electrode to the counter electrode, which is usually made of a highly conductivity materials, such as platinum.

Biocatalytic and Affinity Electrochemical Sensors

Electrochemical biosensors can use recognition elements, such as, antibodies, nucleic acids, proteins, enzymes, tissue slices, etc., and can be grouped into two important categories: biocatalytic and affinity sensors[127].

Biocatalytic sensors are commonly used for protein detection using enzymes as the principal recognition element, due to their high biocatalytic activity, affinity to biorecognition and signal amplification, and substrate specificity. These unique properties offer a biological detection process that is cheap and easy to implementation[128]. For these sensors, the probe or working electrode must be coated with a thin layer of an immobilized enzyme that has to be replaced periodically according to the electrode's lifespan. Common immobilization techniques include enzyme entrapment, encapsulation, incorporation, adsorption, cross-linking, and covalent attachment[129, 130, 131].

Affinity Sensors are based on strong and selective binding events between a biological recognition element, such as antibodies (Abs), membrane receptors, and oligonucleotides, and the target analyte. Here, the recognition process depends on size and shape complementarity, between the binding site and the target analyte[132,13,133]. Depending on the biorecognition element that is employed, affinity sensors can be grouped as DNA hybridization and immunosensors. The DNA hybridization-based sensors detect the interaction of a DNA, RNA or aptamer with certain proteins or base-pairing sequence complementarity to immobilized DNA/RNA on the electrode's surface. This sensor is commonly used in medical diagnosis for cancer, viral infections and genetic diseases[134, 135, 136,137]. Immunosensors, on the hand, are based on the non-covalent reaction between an antigen (Ag) and an antibody (Ab). This process is characterized by high specificity and affinity. An Ag is any molecule recognized as foreign in an organism, whereas Ab molecules are produced by specialized cells of the immune system. The Ab must be immobilized on the electrode's surface, using a specific, high catalytic organic label. The most common labels used are GOx, alkaline phosphatase (ALP) and β-galactosidase (β-Gal). Generally, Ab immobilization techniques includes covalent binding, adsorption and biotin-streptavidin linkages[138,139,140].

A key factor that affects the sensitivity of the immunosensors is the non-specific binding (NSB) interaction between Ab and undesirable molecules. Design strategies to prevent this involves the usage of specific blockers, such as, BSA. Immunosensor applications include food safety, detection of biological toxins, bacteria and virus[141,142,143], as well cancer-specific drugs[144].

Table 1 presents a summary of different electrochemical sensor techniques applied to biosensing.

Table 1. Selected studies on electrochemical biosensors.

Target Analyte	Electrochemical technique	Functionalized probe	LOD	Pros	Cons	Reference
Dopamine	Voltammetry	Graphite/nafion-SPCE	0.023 µmol L^{-1}	Good selectivity and stability	Constrained sensitivity	[145]
Beta-amyloid (Aβ) peptide	Voltammetry	AuNPs/ITO electrode	50 nmol L^{-1}	*In-vitro* highly sensitive sensor	Specificity depends on redox properties	[146]
TNF-α	Voltammetry	TNF-α antibodies	2 fg mL^{-1}	High sensitivity, selectivity, stability and reusability	Low portability	[147]
SARS-CoV-2	Voltammetry	Spike antibody-graphene oxide (f-GO) modified glassy carbon electrode	1 ag mL^{-1}	High specificity, sensitivity and fast detection time.	Low potability	[148]
Prostatic specific antigen (PSA)	Amperometry	Ab-AuNPs-HRP	0.2 ng L^{-1}	Rapid and sensitive detection	Non repeatability consideration	[149]
HER2	Amperometry	CD24c/AuNPs-GO/GCE	0.23 nmol L^{-1}	Early analyte detection	Non-specific current appearance	[150]
Cardiac troponin I (cTnI)	EIS	Anti-cTnI-PtNPs/Graphene-MwCNTs/GCE	1 pg mL^{-1}	High sensitivity and selectivity	No reported	[151]
SARS-CoV-2	EIS	Spike (S)	1.065 fg mL^{-1}	High sensitivity and selectivity, low-cost, portable, rapid diagnosis	Electrode repeteability.	[152]
Testosterone	EIS	Molecularly imprinted polymer/graphene-oxide (MIP/GO)	0.4 fmol L^{-1}	Good selectivity and long-term stability	No reported	[153]

Perspectives and current challenges

The use of sensors for biomarker detection continues to attract a growing interest, therefore the search for novel designs with higher sensitivity and selectivity, non-invasive approaches, lower cost and ease of implementation and operation continues. The design of biosensors focuses on improving two major aspects: i) selectivity of target analyte/s and ii) detection technique. The former involves all information related with the analyte and its interaction with the experimental environment. Designers must establish the best possible signals (measurable and distinguishable with high SNR) associated to the interaction between a probe and a given target analyte. On the other hand, the detection method, or transducer, guides costs, ease of implementation, power consumption, reliability, and capabilities for *in-vivo* or *ex-vivo* measurements, etc. A significant part of this effort remains on materials' choices that seek to improve the overall biosensor's sensitivity, LOD, selectivity, measurement range, measurement time and repeatability. State-of-the-art approaches show that the most common biosensors today are based on optical, mechanical, electrochemical and FET principles. Each type with its own advantages and disadvantages depending on the application, as summarized in Table 2. In the medical field, the electrochemical biosensors are preferred for protein detection due to its simpler implementation, high sensitivity (fmol L^{-1} to nmol L^{-1}) and selectivity, low cost and fast chemical response. Moreover, bio-functionalized electrochemical devices can detect a wide range of biomarkers by chemical affinity between the analyte and the electrode's surface material. However, the sensor's performance may be compromised by the type of electrode and its response within the electrochemical technique that is employed. Therefore, the electrode material and functional groups need to be chosen accordingly.

Current research and development efforts on biosensors, seek to overcome the inherent design and manufacturing limits at the nanoscale, by exploiting new techniques, materials, and implementation technologies. Continued research in the field is expected to enable higher levels of technology integration, new bottom-up and self-assembled synthesis, improved portability and power efficiency, higher accuracy and resolution, and faster real-time monitoring capabilities. Biosensors will soon become an integral part of hand-held or embedded devices, e.g., for real-time and non-invasive health monitoring, early disease detection, improved drug delivery systems in disease treatments, for humans, animals and plants alike. Furthermore, biosensors will become essential tools to improve our understanding of, and to optimize the response of living organisms to biotic and abiotic stresses, i.e., to elucidate complex genomic-phenotypic relationships to correlate gene function with gene expression, under different conditions. Biosensors will offer new

ways to study and understand a wide range of biological processes, over multiple length and time scales.

Table 2. Summary of biosensors platforms.

Sensing platform	LOD range	Sensitivity	Pros	Cons	Preferred applications
Optical	1 pg mL^{-1} to 100 µg mL^{-1}	Can be improved using nanoparticles (NPs)	Ultrasensitive analyte detection	Selectivity decreases in complex biological solutions	Environmental biomedical and pH measurement
Mechanical	4 fg mL^{-1} to 20 µg mL^{-1}	Proportional to the molecular mass of the analyte	Mass per area sensitivity can be improved by cantilever geometry	Detection signal can be affected highly affected by non-specific adsorption	Biological and food monitoring
FET	0.04 fg mL^{-1} to 20 mg mL^{-1}	Can be controlled by the channel's electronic transport properties	Ease integration with electronic and portable systems	Short measurement ranges that depend on channel geometry and electrical properties	Environmental measurement, ion detection and IoT devices[151]
Electrochemical	0.4 fg mL^{-1} to 0.023 µg mL^{-1}	Depends on the relation between the chemical affinity among the species and electrode properties	Ease implementation, setup. measurement and characterization	Non-specific binding molecules decreases signal to noise ratio and specificity depends on redox properties	Food Monitoring, pharmaceutical and biomarker detection

Objectives

General Objective

Design non-invasive, portable, and low-cost electrochemical biosensors with improved analytical sensitivity and selectivity for quantifying pathogens and metabolites in humans and plants, enabling real-time, *in-vivo*, and *in-situ* health monitoring.

Specific Objectives

1. Design and implement electrodes, transducers, and a processing single device for the non-invasive detection and monitoring of target analytes in humans (SARS-CoV-2) and plants (glucose and salicylic acid).
2. Optimize the sensitivity and selectivity parameters for the detection of these analytes within a linear measurement range of applicable interest in each case (i.e., 1 fmol L^{-1} to 50 fmol L^{-1} for SARS-CoV-2, and 1 µmol L^{-1} to 500 mmol L^{-1} for salicylic acid).
3. Assess the performance of the biosensors using *in-situ* and *in-vivo* measurements (of humans and plants exposed to different stressors).
4. Demonstrate quantifiable improvements in sensitivity or selectivity, and non-invasiveness, compared to state-of-the-art methods for detecting and monitoring the target analytes.
5. Identify limitations of the designed biosensor in terms of repeatability, linearity, electrode lifespan, and commercialization aspects, providing insights for future research and development.

Materials and Methods

Biosensor Platforms for Human and Plant Health Monitoring

Portable Instrument for Electrochemical Measurements

Figure 2a presents a block diagram illustrating the architecture of the developed instrument. It utilizes an Arduino Nano 33 IoT, featuring a low-power Arm® Cortex®-M0 32-bit SAMD21 processor, 8 ADC channels (8/10/12 bits), and a 10-bit DAC. The instrument also includes a 0.91" OLED display with 128x32 pixels resolution, an integrated AD9833 waveform generation module capable of producing sine, square, and triangular waveforms within a frequency range of 0.1 Hz to 12.5 MHz. Signal conditioning and filtering are carried out using an operational amplifier circuitry (MCP6074). Power is supplied by two 1.5 V AAA batteries, providing approximately 5 hours of continuous operation. To determine this duration, we conducted consecutive measurements using the instrument until the batteries were depleted, and we observed that it was able to complete approximately 25 measurements before the power source was exhausted. A DC-DC converter generates 5 V and -3.3/3.3 V sources, where the 5 V source powers the Arduino unit and the 3.3 V source powers the digital components.

The signal conditioning module adjusts the offset (0 V) to compensate for the open circuit potential (OCP), which represents the initial voltage when no current is flowing, as well as the +/- signal amplitudes. It then applies the potential waveforms produced by the signal generation module to the working electrode (WE), amplifies and filters the current through the WE[154]. Moreover, the signal conditioning module, includes a potentiostat to maintain a constant potential between the reference electrode (RE) and counter electrode (CE) while decoupling the electrodes[155–157]. The operational amplifiers act as buffers for each electrode. Here, the MCP6074 JFET-based operational amplifier allows for high input impedance and low input noise current. To capture ultra-low analyte concentrations (< fg mL^{-1}), with currents in the nA range, we use a trans-impedance amplifier (TIA)[158–161] that provides the current ranges specified in Table 3, while filtering adherent noise[162]. These current ranges can be controlled with the analog switch 74hc4066 using the Arduino. Currents above these ranges are limited (saturated) by the dual +/-3.3 V potential and the low feedback resistance implemented in the TIA operational amplifier. The latter stage in the conditioning module incorporates the 10-bit Arduino ADC unit capable of sampling at 300 ks/s that discretizes the generated waveforms and the output current from the electrodes. Here, the

offset of the output signal form the TIA stage must be adjusted to span it within the range of 0 V to 3.3 V allowed by the ADC.

The PCB is housed in a plastic enclosure that provides support and protection. It includes a 4-terminal electrode connector, enabling the use of 2, 3, and 4 terminal electrodes. Additionally, there is a button-controlled interface to enhance user control and monitoring (refer to Figure 2b). A reusable electrode base, based on a PCB, ensures safe measurements and secure disposal of connected electrodes.

The user interface offers various options, including the Covid-19 diagnosis method, technique selection menu, customization of technique parameters, WiFi connectivity, Micro SD storage, test ID input, and language selection. Before applying the waveform excitation potential between the WE and RE and recording the output current flow, the instrument verifies the presence of an electrode inserted. All input signals undergo digital filtering to reduce noise. The supported electrochemical techniques include cyclic voltammetry (CV), differential pulse voltammetry (DPV), amperometry (CA), and EIS. For the EIS method, the CPU calculates the real and imaginary impedances for each applied frequency, based on Euler's equation (1).

$$Z' = \frac{V}{I} cos\ \Gamma\ ,\ Z'' = \frac{V}{I} sen\ \Gamma \quad (1)$$

A Fourier transform algorithm is implemented to determine the phase difference between the applied potential and the output current. Impedance tuples are used to generate the corresponding Nyquist plot.

Table 3. Signal generation module specifications.

Parameters	Value
Range 1	1 nA – 100 nA
Range 2	100 nA – 1 uA
Range 3	1 uA – 100 uA
Range 4	100 uA – 1 mA

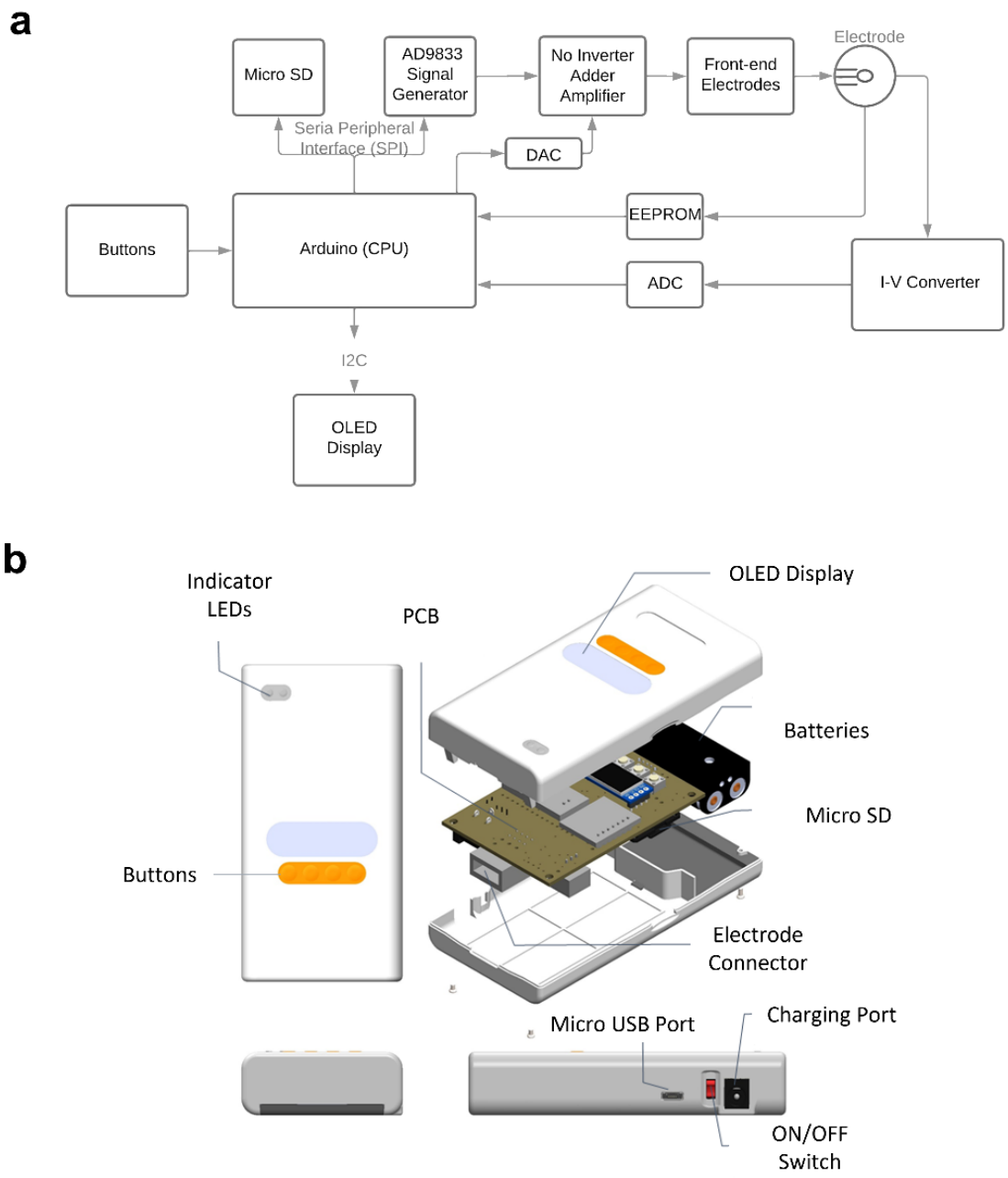

Figure 2. Portable Instrument for electrochemical measurements. a) Block diagram illustrating the components of the instrument. The Arduino serves as the central processing unit (CPU) and controls the generation of signal waveforms using the AD9833 module and the 10-bit DAC. b) Device enclosure showcasing the compact design. The instrument is powered by two AAA batteries and includes a power jack port for easy recharging.

Fabrication and Functionalization of Screen-printed Carbon Electrodes for SARS-CoV-2 Detection

The screen-printed carbon electrodes (SPCEs) were fabricated using a screen-printing thick-film deposition process[163]. The electrodes included a working electrode (WE) with 0.44 cm diameter, an Ag/AgCl pseudo reference electrode, and a counter electrode, all printed on a PET film substrate. The WE and CE were printed using carbon-based conductive paste, while the RE was printed using Ag/AgCl paste. The RE was dried at 120 °C, and the WE and CE were cured at 130 °C. A total of 132 SPCEs were printed on PET sheets, and 15 sheets were produced in a single batch. The electrodes were cleaned using methanol, followed by cyclic voltammetry scans (scan rate = 0.05 V/s, potential = 10 mV) and EIS tests (frequency = 0.02 Hz to 20 kHz, potential = 10mV) to confirm quasi-reversible behavior towards redox species using 50 µl of 1mmol L^{-1} $K_3Fe(CN)_6$ in PBS 1X solution.

For selective detection of SARS-CoV-2 spike protein, the WE's surface was modified by electrodeposition of para-aminobenzoic acid (PABA) through 50 µL diazonium salt in 0.1 mol L^{-1} HCL solution. CV sweeps were performed to ensure proper modification. The PABA-modified WE was washed with distilled water and dried. The PABA-modified WE was chemically activated with 1-ethyl-3-(3-dimethylamino propyl) carbodiimide hydrochloride (EDC) and N-Hydroxysuccinimide (NHS) (0.05 mol L^{-1} EDC and 0.05 mol L^{-1} NHS in 2-morpholinoethane sulfonic acid, sodium salt-MES Na, pH 6.0) for 1 hour at 5 ºC ± 0.5 ºC. A solution of monoclonal antibody (mAb) dissolved in 1X PBS (0.01 mol L^{-1}, pH 7.4) was incubated on the WE for 2 hours. Reference 4015-D003 chimeric Anti-Spike-mAb from Sinobiological was used for spike protein selectivity. To accelerate the EDC-sulfo (NHS) activation process 2-(N-morpholino)ethanesulfonic acid (MES) was used. mAbs bind to the carboxyl end of PABA, preferentially through their lysine residues. The SPCE was then washed with 5 mL of PBS 1X solution and dried at room temperature. To reduce the non-specific binding of other molecules to the surface of the electrode, preventing unwanted interactions and reducing background noise, a 1% concentrated solution (10 mg mL^{-1}) of bovine serum albumin (BSA) was dissolved in a sodium salt (0.5 mol L^{-1} MES) buffer solution at pH 6.0 and incubated on the WE for 1 hour at room temperature. The SPCE was then washed again with 5 ml of PBS 1X solution and dried at room temperature, before use or preservation in a 4 ºC humid environment.

Fabrication and Functionalization of Screen-printed Carbon Electrodes for Glucose Monitoring in Plants

Glucose sensors were fabricated using a screen-printing process with a semiautomatic MMP-SPM printer (Speedline Technologies, Franklin, MA, USA). The metallic steel stencils compatible with this printer were manufactured by engraving the electrode design drawn on AutoCAD 2018 software (Autodesk, San Rafael, CA, USA) onto 12 in. x 12 in. and 75 μm thick stencils by Metal Etch Services, San Marcos, CA, USA. Thus, the three-electrode system consists of a working electrode (WE) with 0.3 cm diameter, an Ag/AgCl pseudo reference electrode, and a counter electrode fabricated using stencils with two different designs with the layer-by-layer screen printing method. In this context, Ag/AgCl patterns were printed on the PET substrate as interconnection and reference electrode, then curing was applied for 10 min at 85 °C. Afterward, working and counter electrode patterns were printed with Prussian Blue carbon ink, and curing was used under the same conditions.

The enzyme-based modification applied to the Prussian Blue WE transducer area (0.07 cm^2) of the electrodes was carried out with a single-layer drop-casting method. First, stock enzyme solution was prepared, dissolving 40 mg mL^{-1} GOx and 10 mg mL^{-1} BSA in 0.1 mol L^{-1} PBS (pH 7.4). Then, the drop-casting solution was formed by mixing the stock enzyme stock solution, 0.1% Nafion, and Glutaraldehyde 1 wt. % in H_2O in a ratio of 1:1:0.33 respectively. Therefore, the modification process was completed by taking 3 μL for each WE from this mixed solution. After completing all these procedures, the electrodes were stored at 4 °C overnight to allow them to dry. The dried electrodes continued to be stored under the same conditions before testing.

Fabrication and Reaction Mechanism of Laser-induced Graphene Electrodes for Salicylic Acid Monitoring in Plants

LIG electrodes were fabricated using a MUSE 3D (Full spectrum laser, USA) laser machine equipped with a 45 W CO_2 laser (λ = 10.6 μm). Graphene was induced onto a 125 μm-thick polyimide (PI) substrate with a parameter configuration of 10% (4.5 W) power and 15 cm/s raster speed[164]. Prior to laser exposition, the substrate was cleaned with ethyl alcohol and thermally treated in an oven at 180 °C for 15 minutes. To reduce thermal deformation caused by the laser the PI substrate was coupled to a 130 μm-thick adhesive vinyl sheet. Then, the LIG

electrode consists of a rectangular graphene-induce working electrode with 0.18 cm^2 effective area (0.3 cm x 0.6 cm), a graphene-induced reference electrode, and a counter electrode with 0.36 cm^2 effective area. CE electrode was covered with Ag/AgCl ink to improve the kinetics of the electrochemical reaction and facilitate the mass transfer of SA to the electrode surface, then curing was applied for 10 minutes at 85 °C. Two connection terminals were added to the WE to ensure compatibility with 3 and 4 electrode connectors.

Salicylic acid was detected through its electro-oxidation process. Since this reaction is irreversible and pH dependent, all measurements were performed in 1X PBS buffer (0.01 mol L^{-1} at pH 7.4). Under neutral pH conditions, the electrochemical oxidation of salicylic acid occurs via a one-electron transfer process[165]. As result, the hydroxyl radicals formed on the electrode surface during the oxygen transfer reactions of water oxidation causes the hydroxylation of SA to form 2,3-dihydroxybenzoic acid, 2,5-dihydroxybenzoic acid and other SA based dimeric products[48]. The large surface area of LIG provides numerous active sites for the adsorption of salicylic acid molecules, thereby enhancing the reaction kinetics[51].

Iontophoretic Electrodes and Hydrogels Fabrication

The iontophoretic electrodes (anode and cathode) were designed on AutoCAD 2023 software (Autodesk, San Rafael, USA) with an effective area of 2.65 cm^2 and then fabricated by cutting a substrate (PET or PI) film with the Cricut Maker 3 machine. Subsequently, Ag/AgCl ink was printed onto the electrodes, and three layers of ink were applied, each cured at 85 °C for 10 minutes. These electrodes were then stored in a petri dish under room conditions. Agarose hydrogels were created by dissolving 3% (w/v) agarose in 0.1 mol L^{-1} PBS buffer. The solution was stirred at 150 °C with a constant rotation speed of 100 rpm until it became transparent. An acrylonitrile butadiene styrene (ABS) mold consisting of circular discs with a diameter of 3 cm and a thickness of 500 µm was used to give the desired shape to the solution. Next, 600 µL of agarose gel solution was transferred for each circular disc to these cavities. The gels that hardened at room temperature were then stored at 4 °C for future use. PVA hydrogels were created by mixing 10 g of 0.1 g mL^{-1} PVA solution, 14 g of 0.2 g mL^{-1} KOH, and 2.6 g of 1.3 g mL^{-1} sucrose. The resulting solution was transferred to a mold with shapes corresponding to the effective sensing area of the sensing electrode and approximately 0.1 cm thick, then were dried for 12 hours in a vacuum desiccator. Once the drying process was completed, the hydrogels were washed in 0.1 mol L^{-1} PBS buffer until the hydrogel pH reached approximately 7.4. The PVA hydrogels were

stored in 0.1 mol L^{-1} PBS buffer at room temperature. Before been used, any excess surface water was removed from the hydrogel using tissue paper.

In-vitro Characterization

SARS-CoV-2 Determination

All SPCEs for SARS-CoV-2 detection were characterized using EIS[166]. Impedimetric measurements were conducted by depositing 50 µL of 1 mmol L^{-1} $K_3Fe(CN)_6$ in PBS 1X solution onto all three electrodes. Impedance measurements were performed at the equilibrium potential of the $[Fe(CN)_6]^{-4}/[Fe(CN)_6]^{-3}$ redox couple with a sinusoidal excitation amplitude of V(t)=0.01 V (RMS). The measurements were taken at 40 steps per decade within the appropriate frequency range (0.5 Hz – 10 KHz), with five repetitions at each frequency, and averaged for each run. The impedance (Z) was expressed in terms of a real component (Z') and an imaginary component (-Z''). On an unmodified WE, the surface is not blocked, allowing the redox probe to easily undergo alternating reactions induced by the AC voltage, V(t).

At each modification step of the WE (4-PABA, mAb, and BSA) and during the testing of SARS-CoV-2(S) antigens, the ions in the redox probe gradually become blocked by bound molecules, resulting in an increase in the charge transfer resistance (R_{ct}) of the interface. The impedance of the WE is influenced by the biological layers that modify its surface. This effect is visualized in a Nyquist plot of real vs imaginary impedance using an AC excitation signal of 10 mV amplitude across the frequency range of 0.5 Hz to 10 kHz. These parameters were chosen to improve the measurement speed and response time of the EIS test while ensuring the recording of all critical data and producing an interpretable EIS response with minimized noise[167]. Each EIS measurement was parameterized using a Randles equivalent electrical circuit model[158] to describe the biosensor-liquid interface. A 50 µl solution of 1 mmol L^{-1} $K_3Fe(CN)_6$ in 1X PBS was employed for this purpose.

To evaluate the performance of the biomodified SPCEs, laboratory sample solutions containing recombinant SARS-CoV-2 spike protein (Reference 40591-V08H, Spike S1-His Recombinant Protein from Sinobiological, USA) were prepared. These solutions covered a concentration range of 1 to 50 fg mL^{-1} and were prepared in 1X PBS. For the experimental procedure, 4 µL of this solution was applied to the surface of the WE and incubated at controlled temperature of 5 ºC ± 0.5 ºC for 5 minutes before performing an EIS measurement. To assess the

in-vitro reproducibility of the sensor, three replicates were included as error bars in the calibration curve, ensuring good statistical validity.

Glucose Determination

To quantify glucose, first, a stabilization step was performed by adding 60 µL of 0.1 mol L^{-1} PBS buffer to the electrode surface, followed by performing 5 consecutive cronoamperometric scans. The last scan served as the current reference or baseline for the subsequent measurements on the SPCE. Subsequently, different concentrations of glucose (20 µmol L^{-1}, 40 µmol L^{-1}, 60 µmol L^{-1}, 80 µmol L^{-1}) were applied, and each one was characterized by performing another 3 CA scan. The last current scan was then compared to the baseline, and the current difference (Δi) between the baseline and the recorded current response at 60 seconds was calculated. These Δi values for each specific concentration were used to construct the calibration curve of the sensor. The CA measurements were conducted using a reduction potential for glucose of -0.15 V for a duration of 60 seconds using the Palmsens4 potentiostat. To assess the reproducibility of the sensor, three replicates were included as error bars in the calibration curve, ensuring good statistical validity.

Salicylic Acid Determination

The electro-oxidation process of salicylic acid can result in the formation of poly-SA films on the electrode surface through coupling and cross-linking reactions. These films can cause fouling, leading to decreased accuracy, precision of subsequent reactions, and reduced electrode reusability. To mitigate this issue, the use of strong bases such as NaOH has been employed to non-destructively remove the poly-SA films from the electrode surface[165]. To ensure accurate measurements and enable electrode reusability, a post-reaction treatment was implemented. After each SA oxidative reaction, 60 µL of 0.1 mol L^{-1} NaOH was drop-casted onto the electrode surface and allowed to sit for 1 minute before being washed away with distilled water.

To quantify salicylic acid, the response of 60 µL of 1X PBS buffer was first stabilized by conducting three consecutive CA scans. The last scan was considered as the current reference or baseline for the LIG electrode. Subsequently, a specific standard concentration of SA (10 µmol L^{-1}, 60 µmol L^{-1}, 150 µmol L^{-1}, 270 µmol L^{-1}, 360 µmol L^{-1}, 550 µmol L^{-1}, 1 mmol L^{-1}) was applied to the electrode surface, followed by another CA scan. The current difference (Δi) between the baseline and the recorded SA current response at 20 seconds was calculated. Each Δi value for each specific concentration was utilized to construct the calibration curve of the sensor. Cyclic

voltammetry studies were conducted to estimate the oxidation peak of SA on the LIG electrodes. The CV measurement was carried out with the potential range from -0.3 to 1.2 V and a scan rate of 0.1 V/s. To assess the sensor's reusability after NaOH treatment, LSV measurements were performed. LSV was conducted from 0.2 to 1.0 V, with parameters including a 0.005 V increment in potential and a scan rate of 0.05 V/s. Salicylic acid concentrations were quantified using CA measurements, in which a constant oxidation potential of 0.8 V was applied for a duration of 30 seconds. All SA *in-vitro* measurements were conducted using 60 µL of 1X PBS buffer media and a PalmSens4 potentiostat and to assess the reproducibility of the sensor, three replicates were included as error bars in the calibration curve, ensuring good statistical validity.

Non-invasive Evaluation

SARS-CoV-2 Diagnosis

The EIS measurement is employed to determine the concentration of spike proteins that have bound to the immobilized monoclonal antibodies (mAbs) on the electrode surface. Prior to detecting the SARS-CoV-2 virus, each electrode used in the process undergoes characterization (blank SPCE with EIS data up to the BSA layer), and the Randles circuit parameters are stored in the SD memory of the instrument. During the diagnosis process, the user enters the pre-defined 9-digit ID of the electrode into the device's GUI. Once the human swab or saliva sample measurement is completed, the implemented firmware compares the newly obtained charge R_{ct} value for the electrode with the previously stored value. If an increase of at least 10% is calculated, a positive diagnosis is displayed on the device's screen.

On-Plant Glucose and Salicylic Acid Monitoring Under Abiotic Stresses

The reverse iontophoretic system applies an electric current between the anode and cathode terminals, creating an electric field that facilitates the transport of biomarkers from the plant to the electrodes through electroosmotic flow. Depending on their charge, different metabolites exhibit distinct migration patterns: neutral and positively charged metabolites move towards the cathode (negative polarized terminal), while negatively charged ones are transported to the anode (positive polarized terminal)[10,43,168]. The ionization behavior of salicylic acid is influenced by pH. Under acidic conditions, salicylic acid exists primarily in its neutral form, whereas in alkaline environments, the carboxylic acid group can lose a proton, resulting in the formation of the negatively charged carboxylate ion (salicylate)[169]. In plants, most SA and its constituents exist in the pH range of 5.0 to 8.0. Under these conditions, salicylic acid exists

predominantly as negatively charged salicylate ions[170]. Consequently, the sensing LIG electrode was positioned in the anode terminal of the iontophoretic system to detect the anionic form of salicylic acid extracted from the leaves. Conversely, due to the neutral charge of the glucose molecule (with balanced positive and negative charges), the SPCE was placed in the cathode terminal.

The utilization of reverse iontophoresis for non-destructive metabolite extraction and identification in plants has been explored in previous studies[168,170]. However, the extended extraction time required to obtain usable volume samples for electrochemical analysis (> 1 h) has hindered the practical application of this technique for plant sensing, considering that the temporal resolution of measurements should be shorter than the biological processes of interest[171–174]. To overcome this limitation, an agarose hydrogel layer was incorporated between the iontophoresis electrodes and the plant's leaf surface to enhance electron transfer at the interface. Additionally, a porous PVA hydrogel membrane was integrated to facilitate the diffusion and absorption of glucose into the working electrode. Implementing a magnetic sandwich setup ensured constant pressure on the leaf surface, effectively reducing the reverse iontophoresis time to just 10 minutes.

The sensor's cathode and anode terminals were strategically positioned on the abaxial and adaxial planes of the leaf surface[168], using magnetic holders in a sandwich-like configuration. This setup effectively reduces the required current intensity for fluid extraction from the plant by minimizing the resistance between the sensor terminals. Each experiment utilized a single designated leaf, and no more than one leaf was involved in a stress experiment. The on-plant measurements followed the following procedure: i) prior to reverse iontophoresis application, the sensor response was stabilized by conducting 15 to 20 consecutive amperometry scans until a consistent current was achieved, with the final scan serving as the current reference or baseline, ii) reverse iontophoresis was then initiated using the anode and cathode electrode terminals, iii) one new amperometry scan was performed after reverse iontophoresis, and iv) the current difference (Δi) between the baseline and the post-reverse iontophoresis value was calculated at 20 seconds for salicylic acid and 60 seconds for glucose. To validate the results, each studied metabolite was also measured without the reverse iontophoresis step. After a 10-minute waiting period, five consecutive chronoamperometry scans were conducted, and the last scan was used to calculate Δi. Additionally, for glucose measurements, control experiments without the enzymatic modification step were carried out. Reverse iontophoresis studies were conducted using a current magnitude of 0.53 mA for 10 minutes, employing the Palmsens4 potentiostat.

Chronoamperometric measurements were performed with a constant oxidation potential of 0.8 V applied for 30 seconds to detect salicylic acid and a reduction potential of -0.15 V for 60 seconds to detect glucose.

Different plant species were utilized to evaluate glucose and salicylic acid under abiotic stress conditions. Glucose analysis was conducted on *Capsicum annuum L.* (sweet pepper), *Gerbera jamesonii* (gerbera), and *Lactuca sativa L.* (romaine lettuce) plants subjected to light and temperature stresses. Salicylic acid measurements were performed on *Persea americana Hass* (avocado) plants exposed to abiotic and salinity stresses. These plants were chosen because they have a leaf surface area > 7 cm^2, which fits the sensing platform comfortably. To induce light stress, plants were subjected to prolonged darkness (> 3 consecutive days) to observe the behavior of endogenous glucose. Additionally, glucose response was monitored using different light bulbs with the same specifications as the study by[175,176] (fluorescent lamp: 10 W/21397, 400 nm – 700 nm, *Goodwill*; blue: 9W/A19, 430 nm, *Gonhom*; red: 9W/A19, 670 nm, *Gonhom*) placed 30 cm from the top of the plant to ensure consistent and evenly distributed irradiance[177]. For temperature stress, glucose levels were monitored in plants exposed to room temperature (25 ºC) as well as two extreme temperatures (10 ºC and 40 ºC) for a duration of 40 minutes. During all glucose experiments, plants were regularly watered with 400 mL per week. In the case of salicylic acid, three avocado plants were included: one under no stress (control), one under salt stress, and one under drought stress. The plants were watered twice a week with 500 mL of water prior to the start of salicylic acid monitoring tests. The drought stress plant did not receive water for 10 consecutive days, starting from the beginning of the salicylic acid measurements. For salt stress induction, the corresponding plant was regularly watered with distilled water containing varying concentrations of NaCl (5 mmol L^{-1}, 15 mmol L^{-1}, and 50 mmol L^{-1}) for 10 days. All measurements were conducted on the same leaf of each plant every 24 hours, maintaining consistent environmental conditions at 25 ± 0.5 ºC. Following each stress measurement, the sensor was easily removed without causing any damage to the leaf, which was then rinsed with distilled water.

Results and Discussion

Electrochemical SARS-CoV-2 Detection using mAb Modified SPCEs and the Developed Potentiostat Instrument

By fitting the curve obtained for each EIS to an equivalent Randles electrical circuit model, it was possible to estimate the charge transfer resistance (R_{ct}), the double layer capacitance (C_{dl}) and the ionic solvent's resistance (R_s). Figure 3A illustrates the fitted curve for a SPCE modified up to BSA using Matlab, and Figure 3B represents the equivalent Randles model.

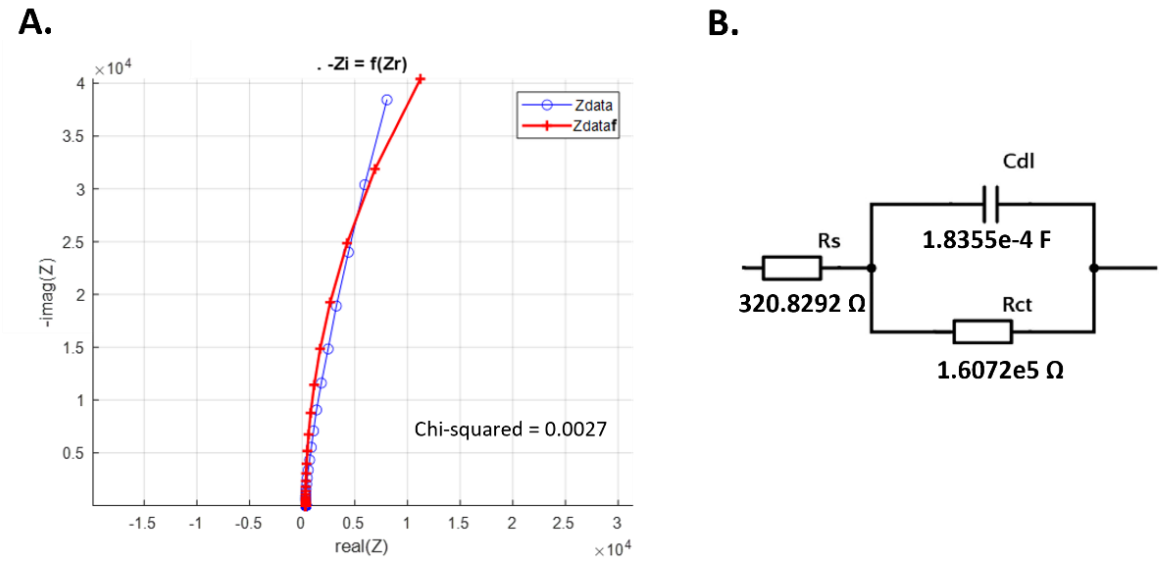

Figure 3. EIS equivalent circuit estimation. A) Fitted curve for a BSA-modified SPCE. B) Equivalent Randles model depicting the estimated R_{ct}, R_s and C_{dl} based on the EIS analysis.

To evaluate the performance of the developed electrochemical instrument using biological samples, a comparison was made between the obtained EIS results of different SPCEs incubated with liquid samples. The measurements were conducted using the developed device (dubbed SenSARS), Autolab, and Palmsens4 potentiostats, all set to the same EIS parameters.

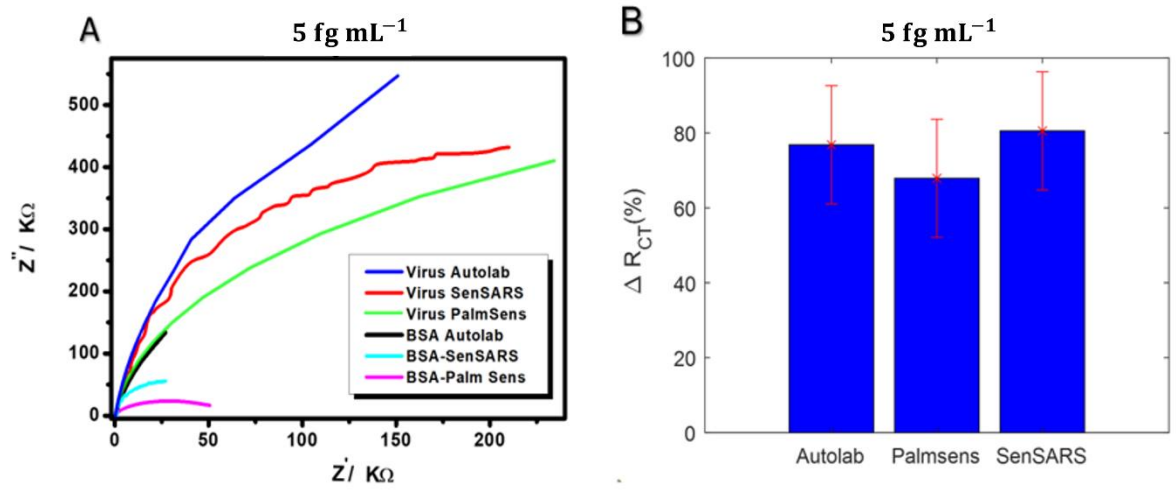

Figure 4. Comparison of electrochemical impedance spectroscopy results. A) EIS comparison between SenSARS, Palmsens4, and Autolab's PGSTAT128N potentiostats for a SPCE modified with bovine serum albumin (BSA), and the same electrode's response with SARS-CoV-2 spike protein at a concentration of 5 fg mL^{-1}. B) Comparison of relative ΔR_{ct} values obtained from EIS measurements on different SPCE electrodes at a concentration of 5 fg mL^{-1}.

In Figure 4A, the EIS test results obtained by the custom-designed instrument, Palmsens4, and Autolab systems are displayed for various electrodes. Each electrode was functionalized with BSA and incubated with a PBS fluid matrix sample containing SARS-CoV-2 (S) antigen at a concentration of 5 fg mL^{-1}. The results illustrate the performance of the different systems for the given experimental conditions. Figure 4B presents the corresponding percentage change in R_{ct} for each pair of BSA-functionalized electrodes and spike protein-functionalized electrodes. The changes in R_{ct} values, denoted as ΔR_{ct}, were calculated by subtracting the R_{ct} value of the BSA electrode from that of the electrode functionalized with the spike protein.

To determine the sensor's dynamic range for SARS-CoV-2 detection, a calibration curve was constructed by adding successive concentrations of recombinant SARS-CoV-2 spike protein (1 fg mL^{-1}, 5 fg mL^{-1}, 10 fg mL^{-1}, 20 fg mL^{-1}, 50 fg mL^{-1}) on different electrodes. The results are shown in Figure 5, indicating a linear response across the entire virus concentration range of 1-50 fg mL^{-1}. The sensitivity of the sensor, represented by the slope of the calibration curve, was determined to be 7.5 MΩ/fg mL^{-1}, and the LOD was found to be 1.065 fg mL^{-1}, which was calculated from LOD=3.3σ/S, where σ is the standard deviation of the response (Table 4) and S is the slope. Figures 5A and 5B illustrate the linear response observed with increasing spike protein concentrations. As the concentration of the virus in the sample (spike protein content) increases, the charge transfer resistance at the electrode's interface also increases.

Table 4. Relative R_{ct} values for different spike protein concentrations and electrodes

SPCE	Stage	Test 1		Test 2		Test 3		σ (Virus)	
		R_{ct} (M Ω)	$\%R_{ct}$	*Rct* (M Ω)	$\%R_{ct}$	*Rct* (M Ω)	$\%R_{ct}$	R_{ct} (M Ω)	$\%R_{ct}$ Virus
1	BSA	1.09	37.43	1.18	33.3	1.09	28.71	0.0852	4.362
	Virus (1 fg mL^{-1})	1.498		1.573		1.403			
2	BSA	1.211	61.76	1.047	93.31	1.081	77.61	0.0525	15.7751
	Virus (5 fg mL^{-1})	1.959		2.024		1.92			
3	BSA	1.06	122.07	1.082	99.81	1,01	127.72	0.099	14.7558
	Virus (10 fg mL^{-1})	2.354		2.162		2.3			
4	BSA	1.046	215.1	1.087	174.33	1.071	142.39	0.3509	36.444
	Virus (20 fg mL^{-1})	3.296		2.989		2.596			
5	BSA	1.18	1219.49	1.022	1342.17	1.082	1376.61	0.6279	82.586
	Virus (50 fg mL^{-1})	15.57		14.739		15.97			

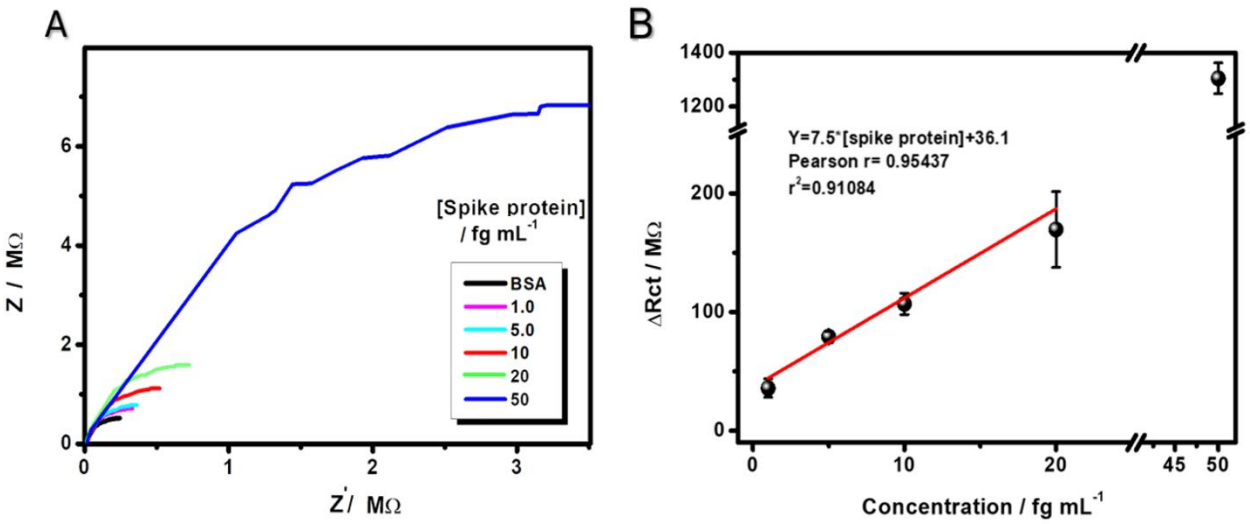

Figure 5. Quantification of SARS-CoV-2 in vitro. A) Relative EIS response with increasing spike protein concentrations in a fluid sample. B) Linear relationship between concentration and ΔRct (change in charge transfer resistance) in the range of 1-20 fg mL^{-1}.

Subsequently, the sensor's specificity was assessed in the presence of potential interferences. The specificity test, as shown in Figure 6, involved measuring the EIS response of an electrode incubated with influenza virus (H1N1) and Epstein-Barr virus (EBV) at concentrations

of 10 and 20 fg mL^{-1}, dissolved in 1X PBS with a pH of 7.4. These potential interfering compounds showed a negligible effect on the spike current signal, with no significant changes observed in the R_{ct}. This high specificity indicates that there are no cross-reactions between the antigens from H1N1 and EBV and the immobilized anti-spike-mAbs, demonstrating the sensor's ability to recognize and respond to SARS-CoV-2 antigens without interference.

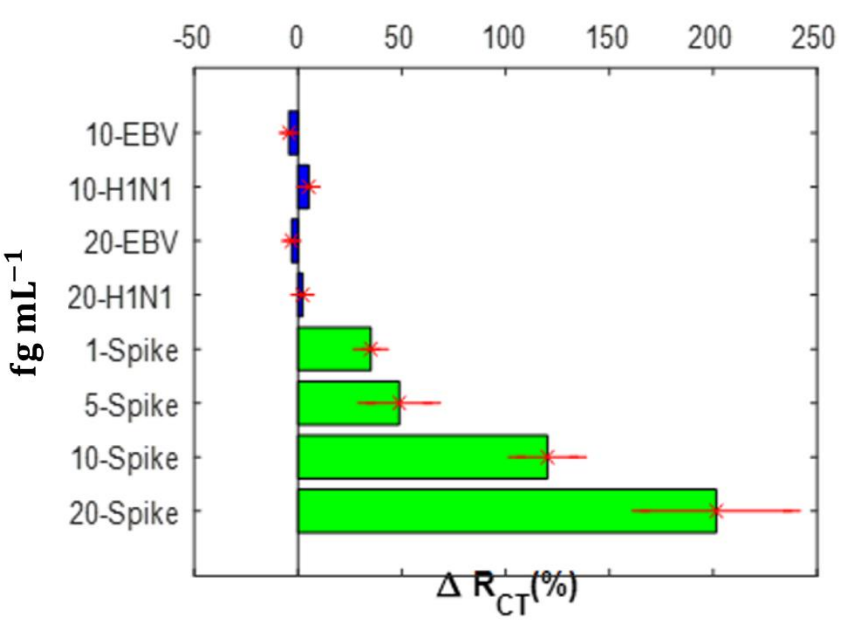

Figure 6. Interference Analysis of SARS-CoV-2 Sensor. Comparison of Relative ΔRct Values for Incremental Spike Protein Concentrations and Negative Control Tests.

Non-invasive, Real-time, *In-vivo* Glucose Monitoring in Plants

Figure 7 presents the non-invasive, non-destructive, and real-time wearable electrochemical biosensor designed for *in-situ* and *in-vivo* detection of glucose extracted from plant leaves through reverse iontophoresis (RI). The sensor is attached to the leaf surface using a sandwich configuration of barium ferrite magnets (0.25 cm diameter and 10 g weight) to ensure easy application and removal (Figure 7a). It consists of two main components: the cathode and anode (Figure 7b). The cathode magnet includes the glucose-selective measurement electrode and the negative terminal of the iontophoretic system, while the anode magnet only contains the positive terminal for iontophoretic application. A low current density (0.2 mA/cm^2) is applied between the anode and cathode through the iontophoresis electrodes to facilitate the molecular flow of plant fluids from the leaves to the measurement electrode. This iontophoretic field induces the

movement of neutral glucose molecules from the anode to the cathode. Within 10 minutes, fluid samples containing glucose are extracted. The sandwich-type configuration allows the sensor to be placed on the leaf surface without causing damage, as the magnets do not exert high pressure (Figure 7c). Additionally, this configuration protects the sensing area from environmental exposure. The overall system integrates a three-electrode screen-printed electrochemical cell configuration, including an enzyme-functionalized working or sensing electrode, a counter electrode, and a reference electrode for glucose sensing. It also incorporates two Ag electrodes (anode and cathode) for iontophoretic extraction of plant fluid, two agarose hydrogels, one PVA hydrogel, medical tape, and two magnetic holders (Figure 7d). The agarose hydrogels act as a protective physical barrier between the leaf and the iontophoretic electrodes, preventing any damage to the leaf. On the other hand, the PVA hydrogel serves as a reservoir and transport scaffold for moving the extracted glucose to the sensing electrode surface. The sensing working electrode is modified with GOx enzyme, which catalyzes glucose oxidation to gluconic acid and oxygen reduction to hydrogen peroxide (H_2O_2). Consequently, glucose can be quantified based on the detection of the H_2O_2 produced. In this case, chronoamperometric detection of the H_2O_2 byproducts is utilized (Figure 7e). The integrated setup was employed to investigate plant glucose levels under different light and temperature conditions (Figure 7f).

In-vitro Characterization

To evaluate the performance and accuracy of the glucose sensor, an *in-vitro* assessment was conducted. The screen-printed electrode was tested with a range of glucose concentrations (20-80 µmol L^{-1}) in 20 µmol L^{-1} increments, using PBS (pH 7.4, 0.1 mol L^{-1}) as the buffer medium (Figure 8a). The results displayed a linear response between current and concentration, as depicted in Figure 8b, demonstrating a sensitivity of 22.7 nA/(µmol L^{-1}·cm²) (equivalent to 1.6 nA/µmol L^{-1}), a LOD of 9.4 µmol L^{-1}, and a LOQ of 28.5 µmol L^{-1}, calculated from $LOD=3.3\sigma/S$, and $LOQ=10\sigma/S$, where σ is the standard deviation of the response and S is the slope of the calibration curve. To assess selectivity, negative control experiments were performed using fructose and sucrose at different concentrations, as these sugars are essential metabolites in plant physiology. The incremental additions of these interfering molecules displayed a negligible (decreasing) response, as illustrated in Figure 8c. This observation further confirms the sensor's high selectivity for glucose detection, distinguishing it from other metabolites commonly found in plants.

Considering the utilization of GOx enzymes as the recognition element, a temperature calibration was conducted to assess the sensor's performance across its operational range of 10-40 ºC (Figure 8b). At lower temperatures (10-25 ºC), the enzymatic activity remained stable, indicating a nearly constant rate of the enzymatic reaction. This stability was attributed to the presence of glutaraldehyde and Nafion coating[178–180]. Glutaraldehyde cross-linking provides a robust physical linkage between the enzyme and the electrode, preventing enzyme detachment and maintaining its catalytic activity. Furthermore, the Nafion coating acts as a protective barrier (hydrophobic layer), shielding the enzyme from environmental factors that may compromise its functionality. Conversely, at higher temperatures, an expected increase in enzymatic reaction rates with glucose resulted in an amplified amperometric signal from the sensor. The temperature effect exhibited a linear relationship within the operational range, which allow to adjust the sensor's calibration curve by a constant factor derived from the temperature-corrected slope difference between the lines in Figure 8b. Notably, the high quality of fit for each calibration curve is indicated by R-squared (R^2) values of 0.9945 for the 25 ºC curve, 0.9768 for the 10 ºC curve, and 0.9845 for the 40 ºC curve. These R^2 values underscore the precision and reliability of the temperature calibration.

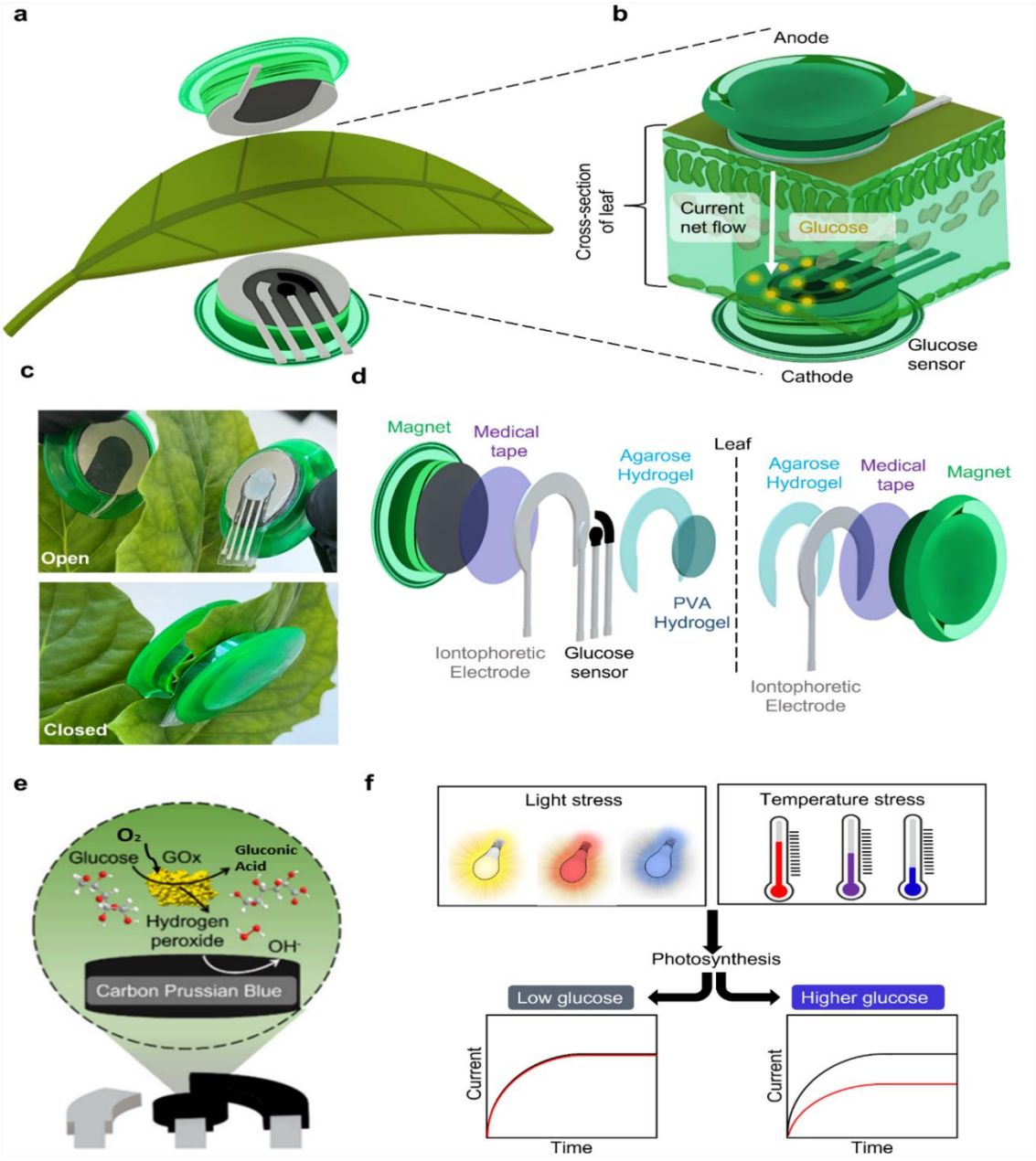

Figure 7. Conceptual illustration of the wearable electrochemical biosensor for plant glucose monitoring. a.) Magnetic clamp assembly on the leaf to secure the sensor. b.) Cross-section illustration of a leaf with clamped sensor inducing a glucose gradient by RI. c.) Clamped sensor mounted on a leaf. d.) Sensor system components and assembly. e.) Glucose recognition mechanism via the GOx enzymatic reactions. f.) Conceptual influence of light and temperature stresses on glucose production (photosynthesis) and its quantification by chronoamperometry. Glucose concentration is determined by the increment of current (red curve) with respect to the baseline (dark curve) of the electrode.

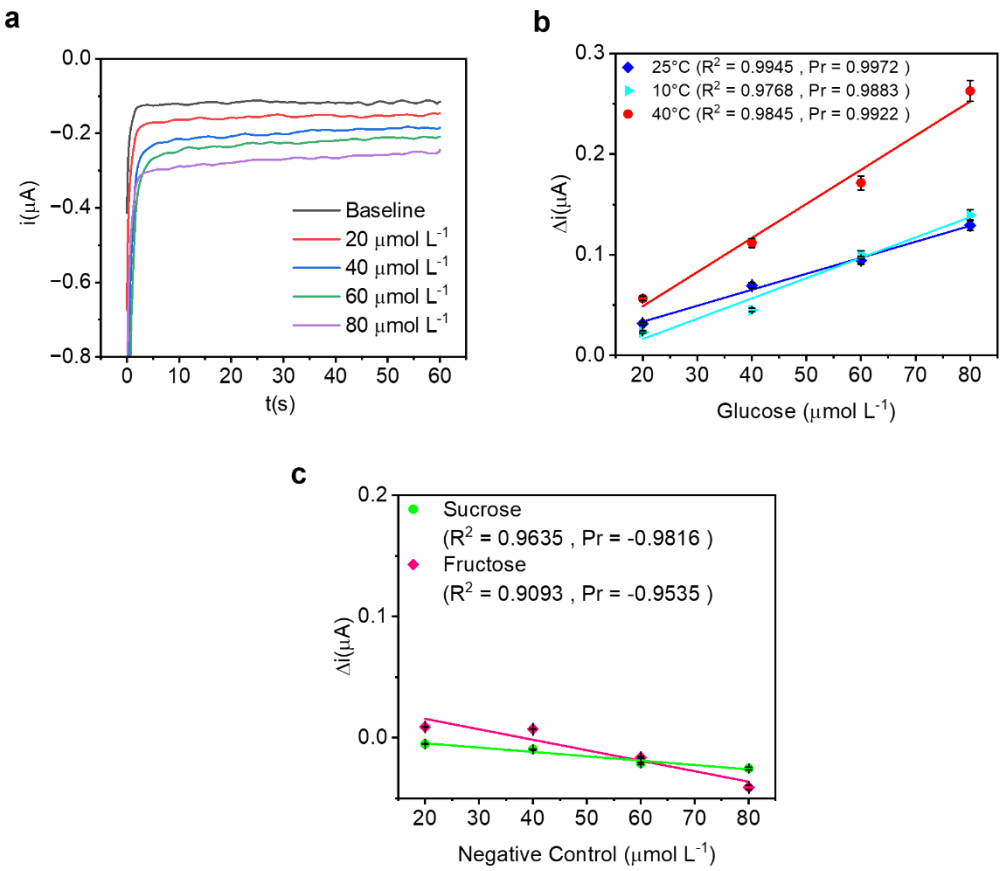

Figure 8. In-vitro sensor characterization. a.) Amperometric response of the sensor for different glucose concentrations (0-80 μmol L^{-1}). b.) Effect of temperature on glucose sensor calibration curves at 25 ºC (dark blue), 10°C (light blue), and 40 °C (red) (LOD=9.4 μmol L^{-1}). c.) Amperometric response of the sensor to possible interfering agents such as sucrose and fructose.

This temperature effect on the sensor's performance can be elucidated by examining its chemical kinetics using the Arrhenius equation. By analyzing the slopes obtained for each calibration curve at specific temperatures (10, 25, and 40 ºC) and the corresponding intercepts, a generalized equation (2) to adjust the sensor's glucose concentration (Gc in μmol L^{-1}) for the entire range of interest (10-40 ºC), was obtained:

$$G_c(T) = \frac{I_s + 2.56x10^{-2} - 1.7033x10^{-4} \cdot T}{1.5x10^{-3} + 4.566x10^{-5} \cdot T} \quad (2)$$

Where I_s is the sensor signal (in μA) obtained after the RI, and T is the temperature (ºC).

In-vivo Control Measurements

To validate the *in-vivo* performance of the sensor as a wearable device for plants, enzymatic and RI control measurements were conducted on the leaf of the plant (Figure 9). In the first experiment, an initial sensor was assembled using a non-modified working electrode (without GOx enzyme) and subsequently mounted on a gerbera leaf. After performing an amperometric stabilization step to establish a baseline, RI was applied for 10 minutes, followed by a sensing step. As shown in Figure 9a, no glucose was detected from the leaf after the post-RI amperometry stage, confirming the requirement of the enzymatic bioreceptor for successful glucose quantification. In the second experiment, a stabilization step was applied to establish a baseline, followed by a waiting time of 10 minutes. The current curves in the post-stabilization step showed negligible glucose detection, confirming the absence of glucose extraction from the leaf without the RI (Figure 9b). Finally, a third sensor with the enzyme-functionalized working electrode was assembled, followed by an amperometric stabilization measurement and 10 minutes of RI. The resulting increase in the current response demonstrated that the combination of both enzymatic bioreceptor and RI steps enables the extraction and subsequent quantification of glucose (Figure 9c).

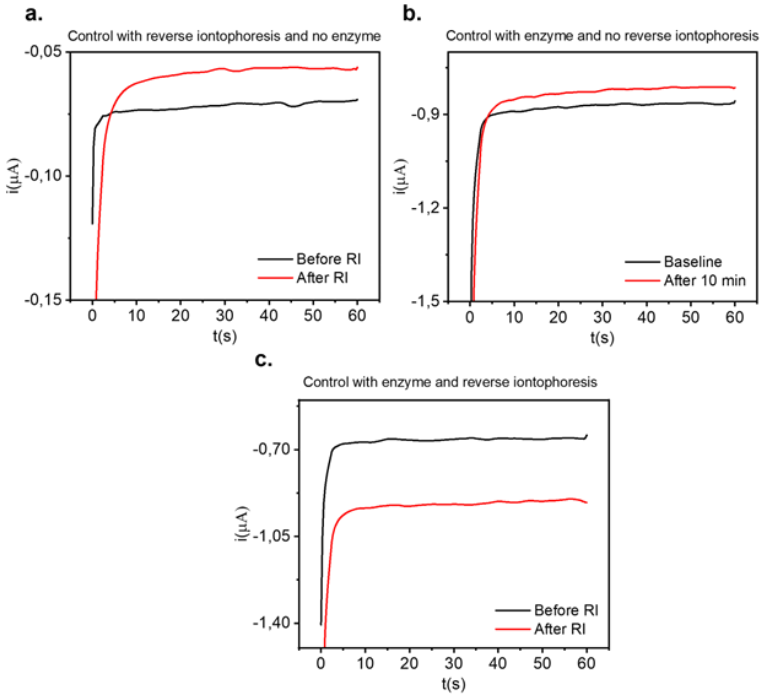

Figure 9. Glucose control tests. a. without sensing system (GOx), b. without the application of RI, and c. with the complete sensing system and the RI application.

In-vivo Glucose Monitoring under Abiotic Stress

To investigate the effect of light on photosynthesis production[181], glucose production was monitored under two stress scenarios: i) a five-day period without light exposure, and ii) a one-hour exposure to three different radiation wavelengths: fluorescent (FL), blue (B), and red (R). In scenario i), a gerbera plant was placed inside a light-sealed box after measuring the initial glucose concentration under standard laboratory conditions (referred to as day 0). Glucose measurements were taken daily at a consistent time (18:00 PT). The plant received a weekly watering of 400 mL, and the temperature inside the box was maintained at a constant 25 °C. The glucose response of the gerbera plant during the 5-day darkness period is presented in Figure 10.

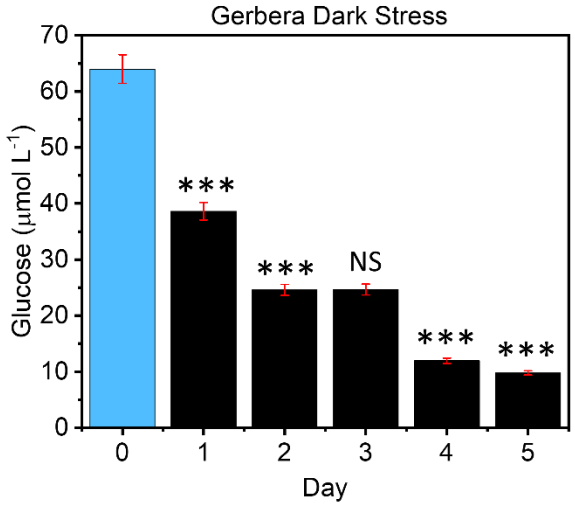

Figure 10. Evaluation of Low-Light Stress in gerbera. Glucose response of gerbera plants during a five-day period of darkness, with weekly watering at a rate of 400 mL and a constant temperature of 25 °C. Statistical analysis was conducted using a T-test, comparing the data to previously obtained results. The significance codes used are "NS" for P > 0.5 (not significant) and "***" for P < 0.001 (highly significant).

In Figure 10, it can be observed that exposing the plant to complete darkness for 120 hours (day 5) resulted in an 85% reduction in its initial glucose concentration (day 0). This decline was expected, as the absence of light inhibits the synthesis of glucose molecules and leads to the gradual consumption of existing glucose for vital biological functions such as respiration[182,183]. The statistical analysis conducted using the T-test revealed significant differences (P < 0.001) in the measured glucose concentrations for days 1, 2, 4, and 5. Interestingly, on day 3, there was no significant difference (NS) observed, and the glucose concentration remained relatively constant (within 5 µmol L^{-1}), indicating the plant's efforts to conserve glucose reservoirs or the

utilization of other carbohydrates to reduce overall energy consumption[184]. After eight days, when glucose levels were entirely depleted, the plant entered an early senescence stage[185,186].

In the second part (ii) of the experiment, the photosynthetic efficiency of three different plant specimens (sweet pepper, romaine lettuce, and gerbera) was studied under three different light wavelengths (fluorescent, blue, and red). Each plant was placed inside a light-free box after establishing the baseline glucose concentration under normal laboratory conditions. After 12 hours of darkness, the glucose concentration was measured, and then the fluorescent light source was turned on for 1 hour. Glucose concentration was measured again, and the light source was turned off. The same process was repeated after 12 hours to evaluate the effects of blue and red light sequentially under identical conditions. The glucose concentrations for each plant under the respective light conditions are depicted in Figure 11.

The results demonstrate that fluorescent light had a significant impact on glucose production compared to the blue and red light sources (Figure 11b-d). The broad spectrum of fluorescent light allows specific frequency bands of photosynthetic pigments to receive more energy, leading to increased glucose production[187]. Statistical analysis revealed significant differences ($P < 0.001$) in glucose concentration increments caused by each light exposure across the three plant models. Each glucose measurement taken without light (dark 1, dark 2, and dark 3 bars in Figure 11b-d) displayed distinct sugar levels after the light stimulus, as confirmed by significant differences ($P < 0.001$) in glucose concentration determined through the T-test. Consequently, each dark measurement served as a reference to calculate the overall increase in glucose concentration or photosynthetic rate resulting from each light effect (Figure 11e). Under fluorescent light exposure, sweet pepper and gerbera exhibited a higher photosynthetic rate (>75%) compared to romaine lettuce, suggesting a more sensitive photosynthetic system that responds to a broad spectrum of light[175,188]. In the case of blue and red lights, gerbera achieved the highest photosynthetic rate[189], while sweet pepper showed the highest rate under red light. Romaine lettuce displayed minor differences between red and blue lights, with a slightly higher photosynthetic rate observed under the latter[190,191].

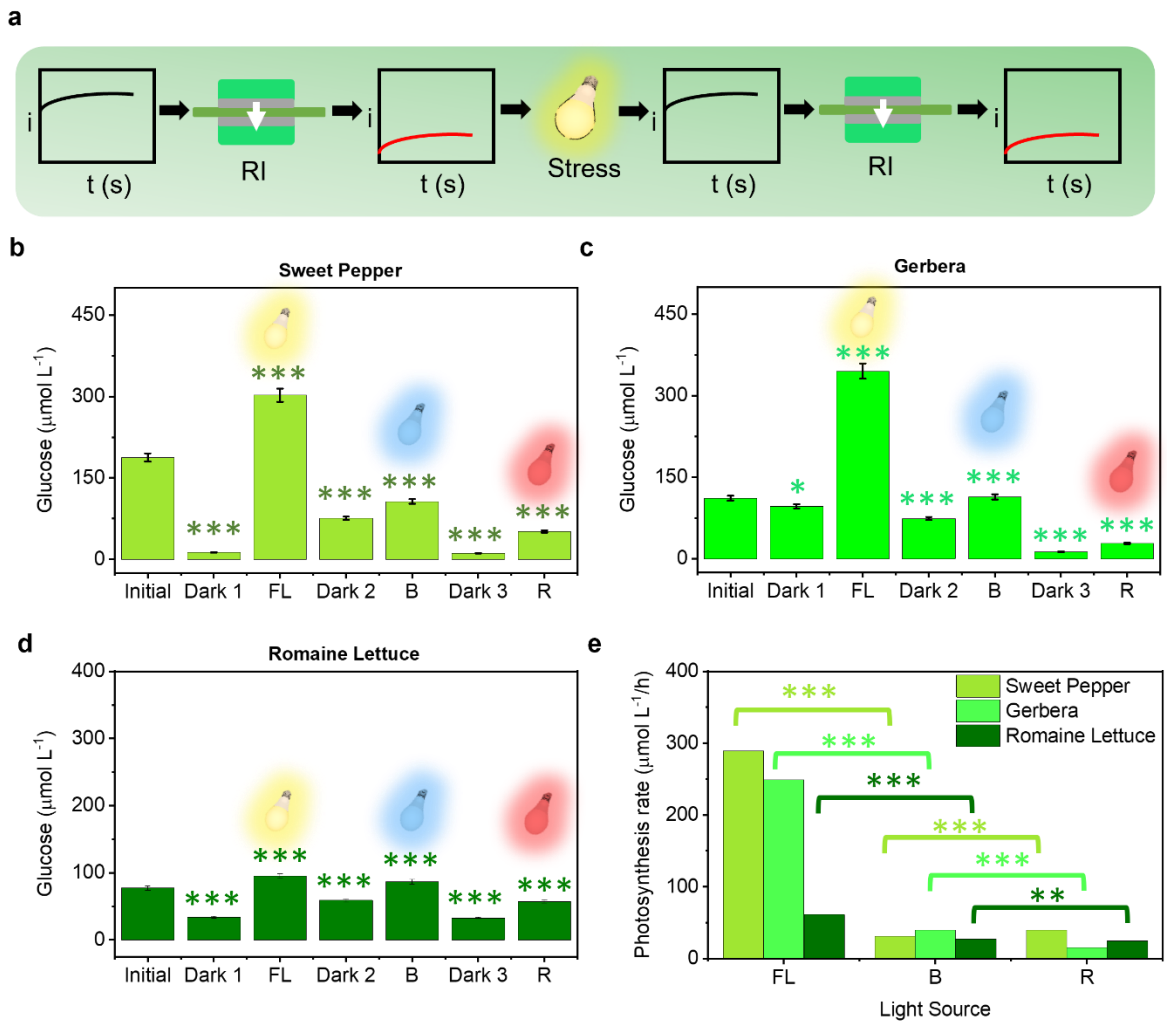

Figure 11. Low-light stress analysis. (a) Protocol for glucose measurement under low-light stress for each plant, measuring glucose levels before and after each light stimulus. The effect of light on photosynthetic response in (b) sweet pepper, (c) gerbera, and (d) romaine lettuce. (e) Calculated rate of photosynthesis for sweet pepper, gerbera, and romaine lettuce under each light wavelength source. Statistical analysis was performed using a T-test with respect to the previously obtained data, and significance codes are as follows: P < 0.05 "*", P < 0.01 "**", P < 0.001 "***".

To assess the impact of temperature on our three plant models, the glucose production at high (40 °C) and low (10 °C) temperatures was further investigated (Figure 12a). Each plant was placed inside a dark room with controlled environmental temperature and received regular watering (400 mL/week). The starting temperature was fixed at 25 °C. After 12 hours, the glucose concentration was measured, followed by an increase in temperature to 40 °C. After 45 minutes of exposure, the glucose was measured under the same settings. Once the sensing step was completed, the plant was left at room temperature (25 °C). To avoid cumulative stress on the

plant, a 24-hour (one-day) recovery step was applied to allow the plant specimen to recover under basal conditions. The same procedure was repeated with a lower temperature (10 °C), with the glucose production measured at 25 °C before the temperature treatment. Figure 12 depicts the glucose response for each plant under the described temperature stress scenario. Glucose values were corrected using the results from the in-vitro calibration curves at each specific temperature (Figure 8b).

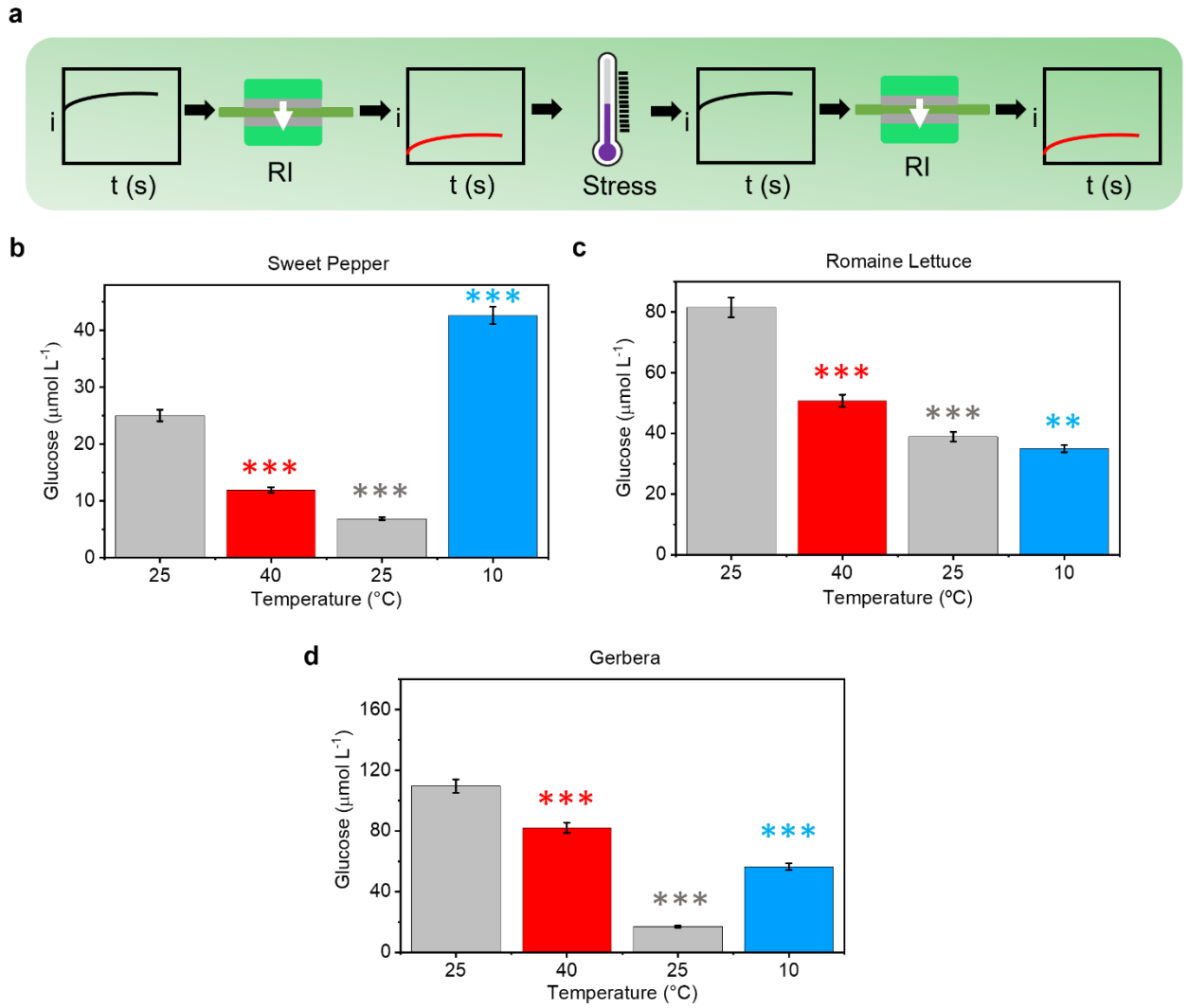

Figure 12. Temperature stress response in three plant models. a) Experimental protocol schematic. Glucose response under temperature stress for b) sweet pepper, c) romaine lettuce, and d) gerbera. Statistical analysis was conducted using a T-test on the collected data. Significance codes: P < 0.01 "**", P < 0.001 "***".

Plants experiencing high-temperature stress respond by initiating stomatal closure to minimize excessive water loss. As a result, the photosynthetic rate is reduced[192] due to the inhibition of ribulose 1,5-bisphosphate carboxylase (Rubisco)[193] and a reduction in intracellular CO_2. Heat stress-induced leaf water loss leads to a decrease in intracellular chlorophyll and carbohydrate content[194]. Consequently, each plant specimen in Figure 12b-d exhibited a significant decrease in glucose concentration ($P < 0.001$) when exposed to higher temperatures (40 °C). Analysis from Table 5 suggests that gerbera exhibits the highest tolerance to temperature variations, as evidenced by the lowest percentage of changes shown in Figure 12d. Conversely, cold-temperature stress triggers sugar accumulation in plants[195,196]. In order to sustain essential biological processes at low temperatures, sugars serve as osmoprotectants[192,197] to safeguard cells from damage and facilitate acclimatization through lipid bilayer contact[198]. From Figure 12b and 11d, it is evident that sweet pepper and gerbera plants displayed a significant increase in glucose concentration ($P < 0.001$) at low temperatures (10 °C), whereas romaine lettuce did not show a highly significant change ($P < 0.01$) (Figure 12c). This observation aligns with the high tolerance of romaine lettuce to low temperatures, as indicated in Table 5.

Table 5. Temperature tolerance for the studied plant species.

	Temperature (°C)		
Plant Specie	Minimum	Optimal	Maximum
Sweet Pepper[199]	18	25	32
Gerbera [200]	16	21	35
Romaine Lettuce [201]	8	20	25

Non-Invasive, Real-time, *In-vivo* Salicylic acid Monitoring in Plants

The wearable device showcased in Figure 13 enables the non-invasive and non-destructive measurement of real-time, *in-situ*, and *in-vivo* salicylic acid levels in plant leaves. The device operates based on the established principles described for the glucose platform (Figure 13a). Extracted samples are directed to an electrochemical sensing LIG electrode, where the oxidative reaction of SA is measured (Figure 13b). Utilizing the negative charge of the SA molecule, the anode magnet is designed to attract the SA molecules through induced electroosmotic flow. To evaluate SA levels, chronoamperometry was employed on avocado plants subjected to two distinct abiotic stress scenarios: drought and salinity (Figure 13d).

In-vitro Characterization

To investigate the electrochemical behavior of SA on the LIG electrodes, cyclic voltammetry was performed. Figure 14a displays the CV curve obtained for 0.5 mmol L^{-1} SA in 1X PBS buffer. The oxidation peak current of SA (I^{ox}) was observed at an oxidation peak potential of 0.8 V. In the subsequent scan, a decrease in the oxidation peak current was observed due to electrode fouling, confirming that this peak corresponds to the SA oxidation process. Additionally, two additional peaks were observed, attributed to the reduction of dimeric SA products (II^{red}) and their consecutive oxidation (III^{ox}) in the second scan[165]. The reusability of the SA sensor was evaluated by washing the LIG electrode with 0.1 mol L^{-1} NaOH after each SA measurement. The electrochemical behavior of the 0.5 mmol L^{-1} SA electro-oxidation process in 1X PBS buffer was measured before and after the cleaning process to ensure complete recovery of electrode surface activity. Figure 14b demonstrates that the electrode surface activity was fully restored with a 1-minute NaOH treatment, showing no significant changes. This highlights the reusability of our LIG sensors and their extended shelf life.

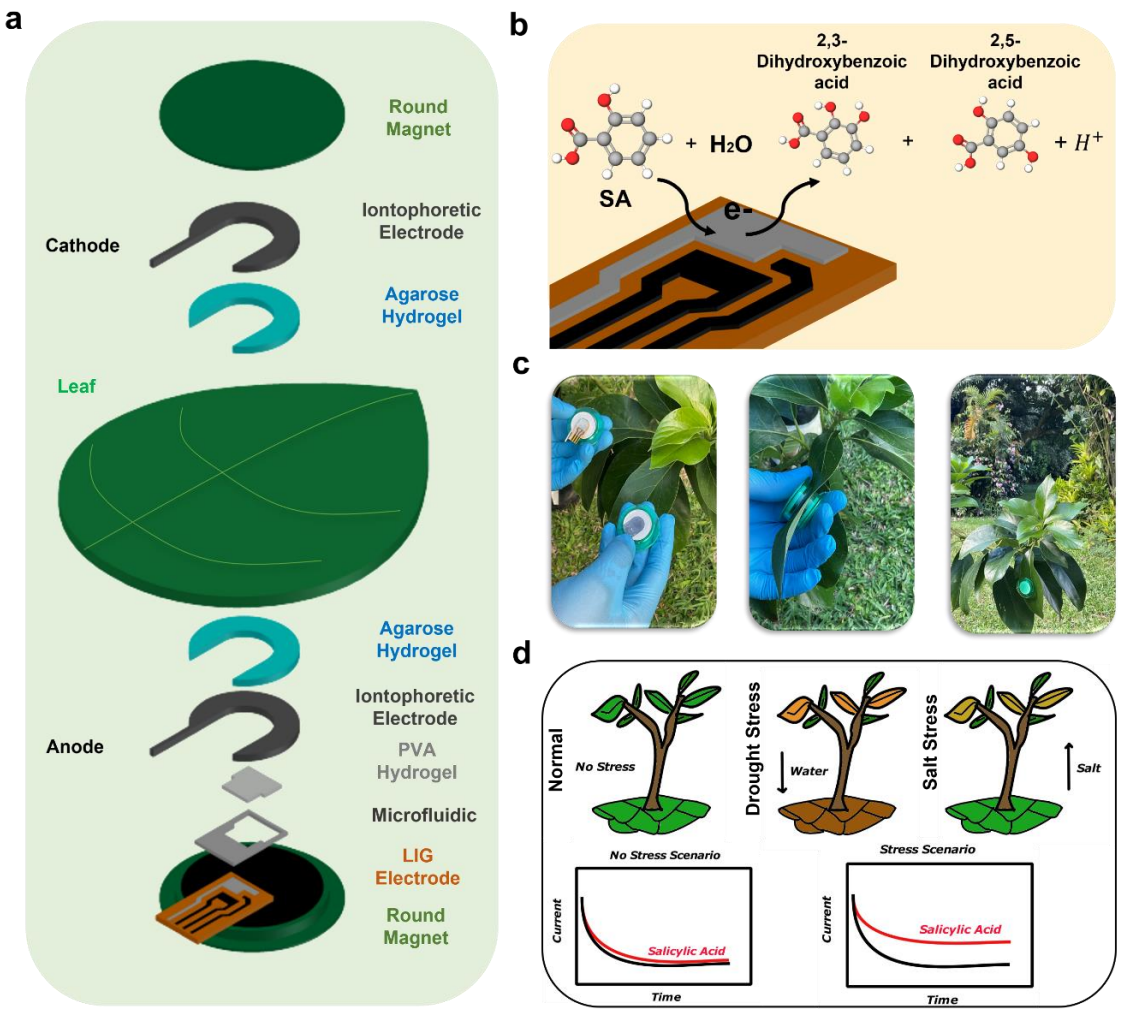

Figure. 13. Wearable electrochemical system for non-invasive salicylic acid monitoring in plants. a) Components of the sensor: The reverse iontophoresis system consists of two silver electrodes and two agarose hydrogels. The electrochemical system includes one LIG electrode as the sensing probe and one polyvinyl alcohol (PVA) hydrogel for sample diffusion on the LIG electrode surface. b) Salicylic acid oxidative pathway: Illustration of the electrochemical reaction involved in the measurement of salicylic acid. c) Sensor assembly demonstration on a plant leaf: The sensor is securely attached to the leaf surface using two barium ferrite magnets. d) Comparison of salicylic acid levels monitored using chronoamperometry in plants under drought and salt stress scenarios, along with a non-stress scenario.

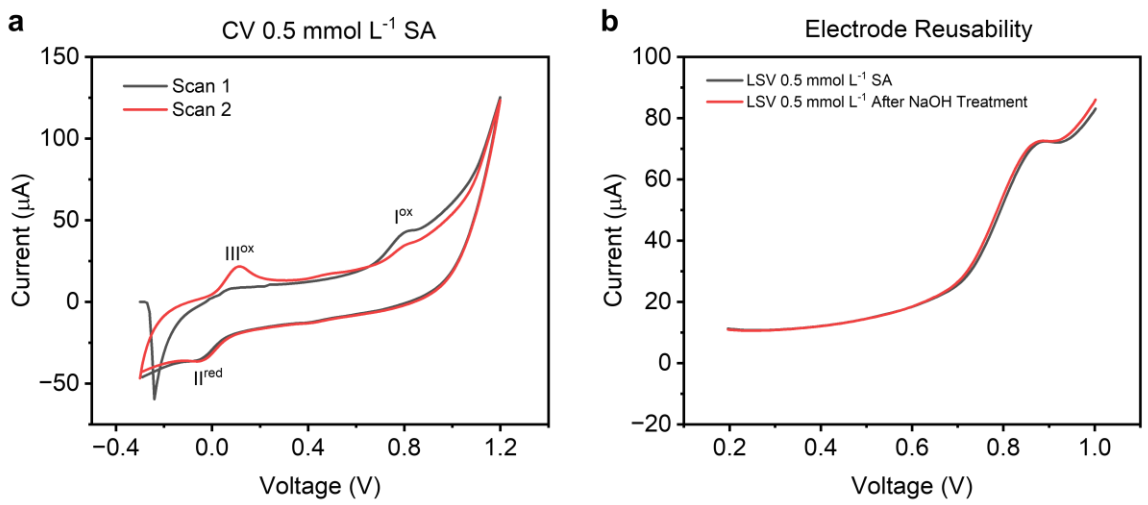

Figure 14. Electrochemical characterization of salicylic acid (SA) on LIG electrodes. a) Cyclic voltammetry analysis of the irreversible electrochemical oxidation of 0.5 mmol L^{-1} SA in 1X PBS buffer, showing the oxidation peak current (I^{ox}) at 0.8 V and additional peaks corresponding to dimeric product reduction (II^{red}) and subsequent oxidation (III^{ox}) in the second scan. b) Evaluation of electrode reusability by comparing the electrochemical behavior before (black line) and after (red line) removing poly-SA films on the LIG electrode using NaOH treatment, demonstrating the restoration of electrode surface activity with no significant changes.

The concentration of SA was quantified using the chronoamperometry method in 1X PBS buffer, covering a concentration range of 10 μmol L^{-1} to 1 mmol L^{-1} (Figure 15a). The response current showed a linear relationship with increasing SA concentration (Figure 15c). The fitted linear equation model for the calibration curve is represented by equation (3). Each replicate used different LIG electrodes. From the calibration curve, a sensitivity of 82.3 nA/(μmol L^{-1}·cm^2) (equivalent to 14.83 nA/μmol L^{-1}), a LOD of 8.2 μmol L^{-1}, and a LOQ of 24.8 μmol L^{-1} were determined from $LOD=3.3\sigma/S$, and $LOQ=10\sigma/S$, where σ is the standard deviation of the response and S is the slope of the calibration curve.

$$SA_C(\mu mol\ L^{-1}) = \frac{\Delta i(\mu A) - 4.3701x10^{-1}}{1.483x10^{-2}} \quad (3)$$

To assess the potential impact of chemical interferences commonly found in leaf samples, a test was conducted to quantify SA in the presence of a mixture of sucrose, fructose, oxalic acid, and citric acid. The concentrations of these interference metabolites were at least ten times higher (200 μmol L^{-1}) than the minimum standard concentration of SA (> 10 μmol L^{-1}) (Figure 15b). The resulting interference calibration curve was compared to the curve obtained for SA without any interferences (Figure 15c). The correlation coefficient was determined to be 0.9996, with only a

2% change in slope between the curves. These results demonstrate that the quantification of SA was minimally affected by the presence of common interference molecules found in leaf samples[168]. The electro-oxidation mechanism at the oxidative potential of 0.8 V selectively targets SA, effectively avoiding the electrochemical activity of other metabolites.

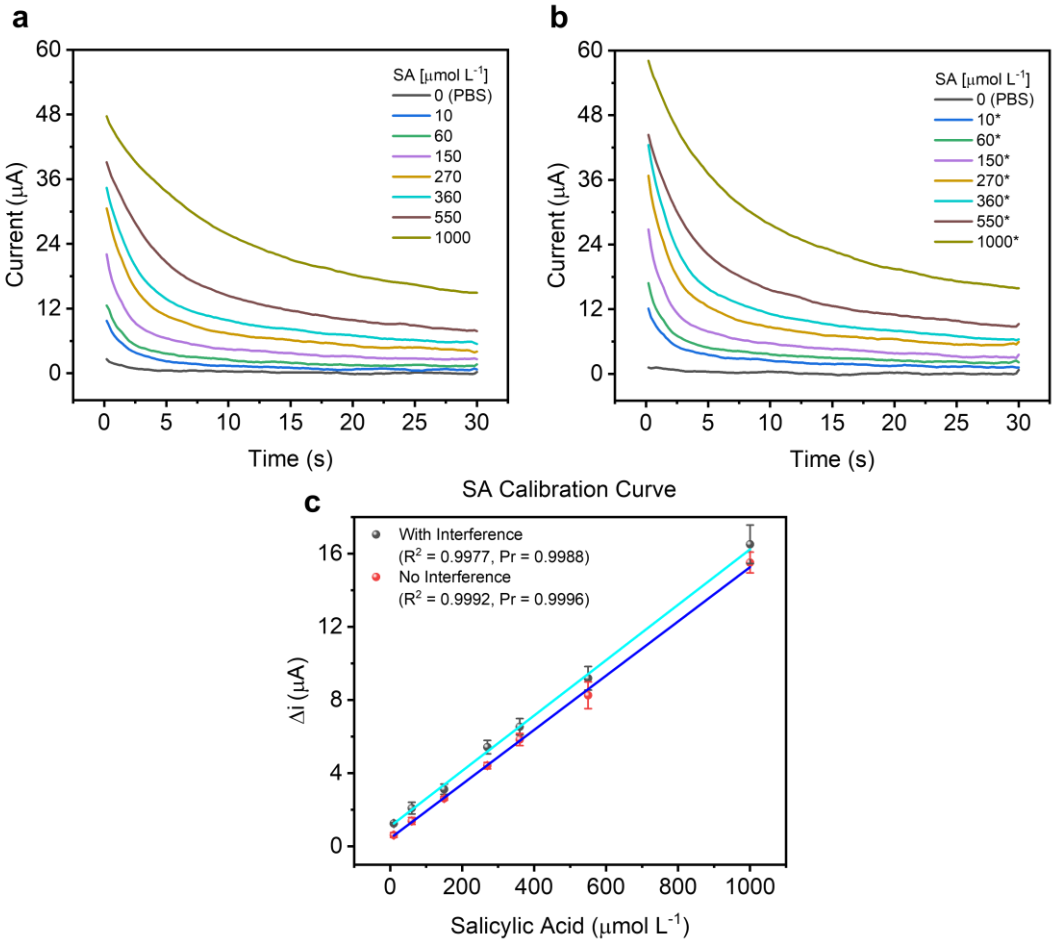

Figure 15. In-vitro electrochemical characterization of the SA biosensor. a) Chronoamperometric response of the sensor for various concentrations of SA (10 μmol L^{-1}, 60 μmol L^{-1}, 150 μmol L^{-1}, 270 μmol L^{-1}, 360 μmol L^{-1}, 550 μmol L^{-1}, and 1 mmol L^{-1}) in 1X PBS buffer without interference. b) Chronoamperometric response of the sensor for the same SA concentrations in the presence of interference (*: 200 μmol L^{-1} sucrose + 200 μmol L^{-1} fructose + 200 μmol L^{-1} citric acid + 200 μmol L^{-1} oxalic acid). c.) Calibration curves for SA quantification with and without interference, demonstrating a high correlation coefficient of 0.9996 and minimal impact of interference on the quantification process.

In-vivo Control Measurements

To validate the *in-vivo* and *in-situ* detection of SA from samples extracted through the RI process, two control tests were conducted on an avocado plant leaf. The first control test involved measuring SA without applying the RI technique. After stabilizing the current with 20 CA scans and a waiting period of 10 minutes, a new set of 5 CA scans was performed. The obtained current curve, as shown in Figure 16a, revealed no detection of SA compared to the baseline, confirming that SA was not extracted from the leaf without RI. In the second control test, the same measurement process was performed with the inclusion of the RI application. After completing the current stabilization step, the RI was activated for 10 minutes, followed by a CA scan. A significant increase in current compared to the baseline was observed (Figure 16b), confirming that RI enables the extraction and quantification of SA from plant leaves.

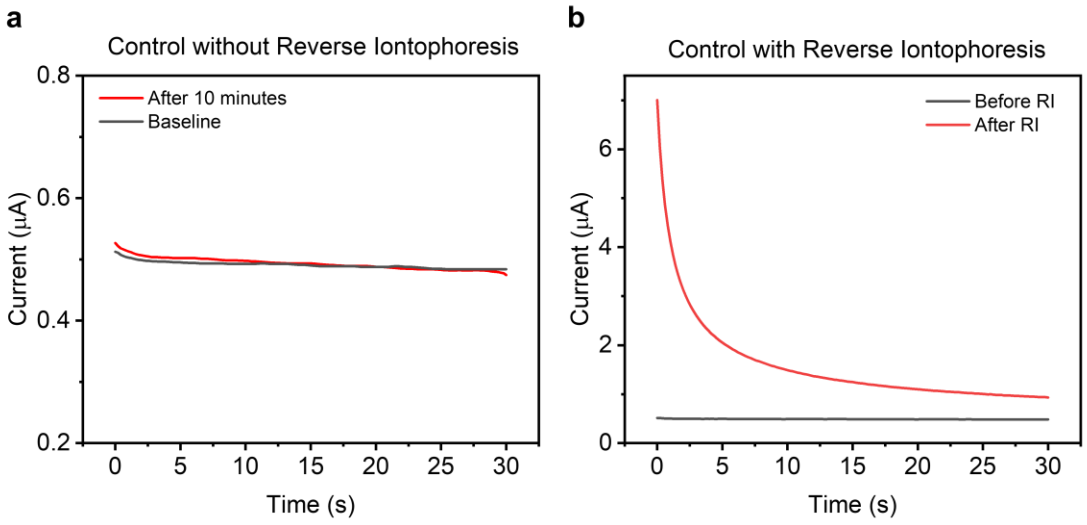

Figure 16. Validation of in-vivo reverse iontophoresis. a) SA determination without RI application. No significant change in current response is observed compared to the baseline. b) SA determination with RI application. A notable increase in the current response is observed after 10 minutes of RI.

In-vivo Salicylic Acid Monitoring under Abiotic Stress

To investigate the effects of drought and salinity stress on avocado plants, the SA levels were continuously monitored for 10 consecutive days. Three plants were assigned to different conditions: i) no stress (control), ii) drought stress, and iii) salt stress. SA levels were measured with a sampling interval of 24 hours, chosen to capture significant changes in SA dynamics while considering the controlled application of stress and the expected gradual response of the plants. The SA response during the 10-day stress monitoring for each plant is depicted in Figure 17.

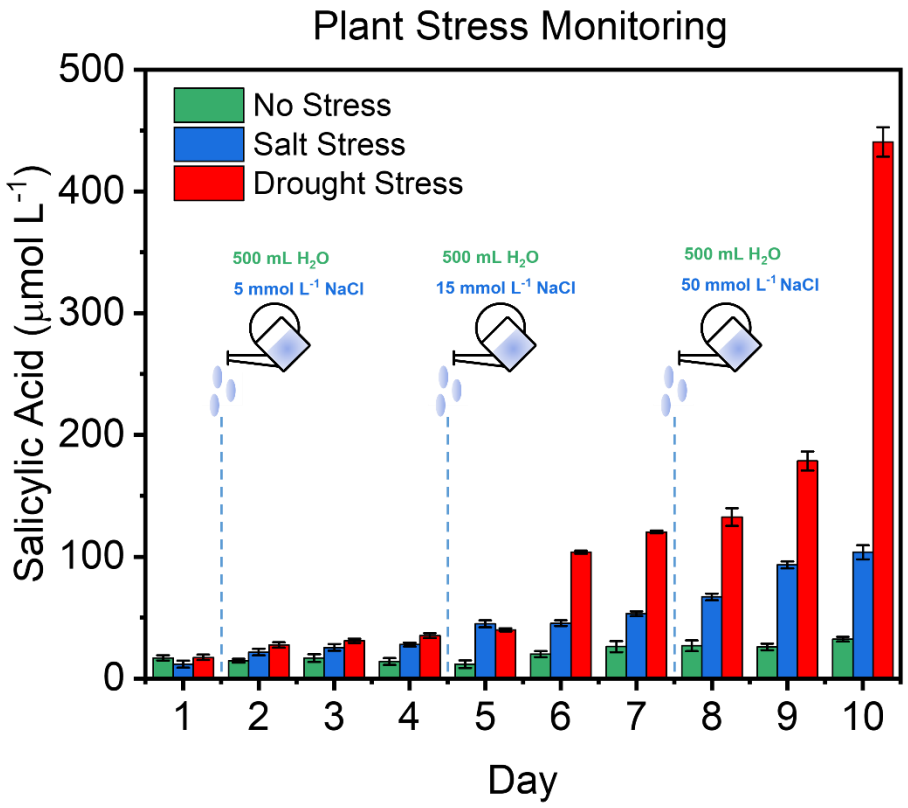

Figure 17. In-vivo monitoring of salicylic acid levels in avocado plants under drought and salinity stresses over a 10-day period. The non-stressed plant serves as a reference for comparing SA dynamics under optimal environmental conditions and during stress scenarios. Increased endogenous SA accumulation was observed under both drought and salt stress conditions, with drought stress exhibiting more pronounced effects.

As depicted in Figure 17, both drought and salt stresses led to the accumulation of endogenous SA in the respective plants, consistent with previous studies[202–205]. Under the salt stress scenario with 5 mmol L^{-1} NaCl, a maximum increase of 16 µmol L^{-1} SA from the initial concentration on day 1 was observed on day 4. Similarly, the drought-stressed plant exhibited a maximum increase of 17.8 µmol L^{-1} SA on the same day. The difference in SA accumulation between these scenarios was only 1.8 µmol L^{-1}. However, the dynamics of SA levels diverged significantly after day 5. On day 6, SA accumulation reached 86.3 µmol L^{-1} in the drought-stressed plant, while in the salt-stressed plant watered with 15 mmol L^{-1} NaCl, the SA concentration increased by 33.7 µmol L^{-1}. Although this was 55% higher than the salt stress level on day 4, it was still 52.6 µmol L^{-1} lower than the value observed in the drought plant. Consequently, the accumulation of SA remained more substantial under drought stress than under salt stress in the

following days. By day 10, the SA concentration had increased by a total of 423.3 µmol L^{-1} in the drought scenario and 92 µmol L^{-1} in the salt-stressed plant treated with 50 mmol L^{-1} NaCl. In contrast, the non-stressed plant exhibited negligible SA accumulation, with only a 15.4 µmol L^{-1} increase from the initial concentration after 10 days. This increase was lower (< 5%) than the final concentrations observed in the stress scenarios.

The pronounced accumulation of endogenous salicylic acid in the plant under drought stress, compared to the plant under salinity stress, can be attributed to several factors. Firstly, water is a crucial requirement for the growth and development of avocado plants[206,207]. Therefore, when a water deficit occurs, it rapidly impacts the plant's health, making it more susceptible to environmental stresses. Secondly, the protective mechanisms activated by the plant to combat drought, such as stomatal closure to reduce transpiration and conserve water, can inadvertently have consequences. The closure of stomata reduces CO_2 uptake, thus affecting the photosynthetic system[202]. As a result, prolonged drought stress can have a more immediate and significant impact on the plant's biological system compared to salinity stress, which is typically a longer-term stressor[208,209]. Lastly, considering that more than 20% of irrigated lands are affected by high salt content, plants have developed more effective mechanisms to combat salinity stress, including the efficient exclusion of Na^+ and Cl^- ions by roots, compared to mechanisms developed to mitigate drought stress[202,210].

Comparative Performance Analysis of the Proposed Non-Invasive Biosensors Against State-of-the-Art Technologies

SARS-CoV-2 Non-invasive Electrochemical Biosensor

The developed device benefits are compared in Table 6 against RT-PCR and other antigen-based technologies.

The time required for diagnosis using the developed system is approximately 10 minutes, with 7 minutes allocated for acquiring electrode response signals to the AC potential excitations, and less than 3 minutes for EIS calculation. This timeframe assumes that the disposable SPCE has been characterized beforehand with a blank solution after bio-modification, and the corresponding EIS is readily available for computing the relative change in R_{ct}. This represents a substantial improvement of 91.67% compared to RT-PCR diagnostics, which typically take 2-3 hours[211], and a 33.33% improvement compared to other relevant biosensor technology that demands 15 minutes for virus diagnosis[213].

Table 6. Key benefits of the proposed platform vs other technologies.

Properties	This Work	RT-PCR	[212]	[213]	[214]	[215]	[216]	[217]	[218]
Viral sample manipulation	NO	YES	YES	YES	YES	YES	NO	NO	NO
Requires trained personal*	NO	YES	NO	YES	YES	YES	YES	YES	YES
Requires specialized laboratories*	NO	YES	NO	YES	YES	YES	NO	YES	NO
Degree of manual sample processing	5%	75 %	0%	> 70 %	> 70%	> 70%	30%	50 %	30%
Time to results	~10 min	2-3 h	30 min	> 30 min	> 30 min	21 min	NA	15 min	30 min
LOD	77 virions (1 fg/ml)	100 virions	10^2-10^3 viruses/ml	10 ng/ml	1 copy/µl	0.1 µg/ml	15 fmol L^{-1}	5 nmol L^{-1}	8 ng/ml
Type of samples	AS, HO, or SA	AS, HO, or SA	AS, HO or SA	Human serum	AS, HO or SA	Cells	AS, HO or SA	Human serum	AS, HO or SA
Selective to	Antigen	RNA	Antigen	Antigen	RNA	RNA	Antigen	Antigen	Antigen
Price per test	< $5	$100	> $10	$8	> $10	> $10	NA	NA	> $10
TRL	TLR 7	TLR 9	TLR 6	TRL4	TLR 9	NA	TRL4	TRL4	NA
Pathogen adaptability	YES	YES	YES	YES	YES	NO	YES	YES	YES
Specificity	>90 %	>96 %	>90 %	>90 %	>90 %	NA	NA	NA	NA
Negative control to other pathogens	YES (EPV, H1N1, rhino)	NA	NA	NA	YES	YES	YES (S1, BSA, E2 HCV, CD48)	YES	YES
Mass producible	YES	YES	YES	NO	NO	NO	YES	YES	NO
Portable	YES	NO	YES	NO	NO	NO	YES	YES	YES
EMI electrode protection	YES	NO	YES	NO	NO	NO	NO	NO	NO
Standalone System⁺	YES	YES	YES	NO	NO	NO	NO	YES	NO

*For usage, not production. ⁺No external devices required for detection. AS: nasopharyngeal aspirate, HO: nasopharyngeal swab, SA: Saliva, NA: not available.

When compared with other technologies, as is shown in Table 6, the proposed system stands out as portable and standalone, eliminating the need for external devices and enhancing its portability. Moreover, it eliminates the need for trained personnel and specialized equipment, making it more accessible for Covid-19 diagnostics. With a LOD of 1 fg mL^{-1} and a specificity of over 90%, provided by the antibody-based detection mechanism, the proposed technology exhibits improved LOD performance (over 23%) compared to the standard RT-PCR diagnostic method and 99.98% improvement against the relevant sensing technology demonstrated in[213]. It's important to note that only a human swab or saliva sample is required for virus diagnosis, and the portable device can process the sample in just 10 minutes. Consequently, invasive samples such as blood or cell extraction are not necessary to quantify low viral loads. Additionally, the overall cost of the instrument is less than $200, considering manufacturing and assembly costs, with the estimated cost per bio-modified SPCE being under $5. This makes the technology scalable for mass production and commercially viable. As a result, this technology enables ubiquitous, rapid, early, and accurate detection of SARS-CoV-2 infections, along with the ability to track viral load over time. These advancements address significant challenges in the diagnosis of this disease[219,220].

Wearable Electrochemical Biosensor for Plant Metabolites Monitoring

The proposed sensing technology for monitoring real-time, *in-situ*, *in-vivo*, and non-invasive response of glucose and salicylic acid in plant leaves encompasses three key innovations. Firstly, it offers non-invasive analyte detection capabilities through a short 10-minute reverse iontophoresis process, enabling the extraction of interstitial fluid from plant leaves. Secondly, it introduces a wearable technology specifically designed for easy placement and removal without causing harm to the plant. Lastly, it enables *in-situ* and *in-vivo* quantification of glucose and salicylic acid, with the potential for adaptation to measure a wide range of analytes or to be applied to various plant species for in-field measurements. The RI process allows for the extraction of plant fluids that contain crucial metabolites of interest in plant physiology[168].

Glucose Biosensor

The key benefits of the proposed plant sensor are compared in Table 7 against other glucose-selective plant biosensors.

Table 7. Advantages of the proposed sensor compared with other glucose-selective plant biosensors.

Glucose Detection	This Work	[221]	[222]	[223]	[224]	[225]
in-vivo (on plant evaluation)	YES	YES	NO	NO	YES	NO
Non-invasive sample extraction	YES	NO	NO	NO	NO	NO
Sensor placement and removal	Magnetic	Stem wound	NO	NO	Microneedle patch	NO
LOD	9.4 µmol L^{-1}	NA	13 µmol L^{-1}	0.01 mg glucose g^{-1} FW	NA	NA
Sensitivity	22.7 nA/(µmol L^{-1} ·cm^2)	NA	11.64 µA/(mmol L^{-1} ·cm^2)	NA	1.22 nA/mmol L^{-1}	NA
Measurement time	< 10 min	< 10 min	< 1 min	< 1 min	< 1 min	< 1 min
Requires trained personal	NO	YES	YES	YES	NO	YES
Requires specialized laboratories	NO	NO	YES	YES	NO	YES
Negative controls to other sugars	YES (fructose, sucrose)	YES (sucrose)	YES (ascorbic acid, fructose)	YES (phenolics, organic acids)	NO	YES (enzyme omitted)
Portable	YES	YES	NO	NO	YES	NO
Detection mechanism	Enzymatic	Enzymatic	Enzymatic	Enzymatic	Enzymatic	Enzymatic
Measurement method	CA	OECT	DPV	CA	CA	OECT
Live plant stress evaluation	Light and temperature	NO	NO	NO	NO	NO

NA: not available, CA: chronoamperometry, DPV: differential pulse voltammetry OECT: organic electrochemical transistor

As shown in Table 7, the developed wearable glucose biosensor exhibits a sensitivity of 22.7 nA/(µmol L^{-1}·cm^2) (equivalent to 1.6 nA/µmol L^{-1}), surpassing the performance of the novel microneedle biosensor designed for *in-vivo* measurements proposed in[220] by at least 130.98%. In terms of LOD, the proposed sensor achieves a value of 9.4 µmol L^{-1}, which is the lowest among the compared sensors and outperforms the microneedle technolog[220] by 99.95%. This outstanding performance is the result of combining an enzymatic bioreceptor (GOx), a carbon-based electrode, and a low reduction potential step (-0.15 V), which enhances selectivity for glucose detection while minimizing responses to interfering molecules such as sucrose and fructose, resulting in a high specificity (>90%) for glucose detection. Notably, this sensor allows the non-invasive extraction of plant fluids through the RI process, making it a pioneering device

for glucose detection and monitoring directly from plants, without the need for invasive extraction procedures —an achievement not reported by any other technology to date (Table 7). Furthermore, its real-time monitoring capabilities enable the study of glucose responses to abiotic stresses, providing valuable insights into the biological processes that regulate sugar levels in stress-tolerant plant mechanisms.

Salicylic Acid Biosensor

A comparison of the key features of the proposed technology against other salicylic acid plant biosensors is presented in Table 8.

Table 8. Key-features comparison between the proposed sensor against other representative SA biosensing technologies.

SA Sensing	This work	[44]	[49]	[226]	[52]	[53]
In-situ/in-vivo detection	YES	YES	YES	YES	YES	YES
Invasive measurement	NO	YES (Microneedles)	YES (Leaf wound)	NO	YES (Microneedles)	YES (Microelectrode)
Sensing method	CA	DPV	DPV	DPV	DPV	DPV
Real-time monitoring	YES	YES	YES	YES	YES	YES
LOD	8.2 µmol L^{-1}	37.4 µmol L^{-1}	0.05 µmol L^{-1}	0.644 µmol L^{-1}	0.14-0.46 µmol L^{-1}	48.11 pmol L^{-1}
Sensitivity	0.01483 µA/µmol L^{1}	0.0001 (µmol L^{-1})$^{-1}$	38.44 µA/µmol L^{-1}	0.002264 (µmol L^{-1})$^{-1}$ (at 0.1 µmol L^{-1})	0.133-0.277 µA/µmol L^{-1}	45 µA/µmol L^{-1}
Selectivity validation	YES (fructose, sucrose, citric acid, oxalic acid)	YES (JA, glucose, ascorbic acid, citric acid, cysteine)	YES (JA, succinic acid, citric acid, ABA, malic acid)	YES (glucose, sucrose, L-tryptophan, L-cysteine, ABA, GA, JA, OA, IAA, citric acid)	YES (glucose, sucrose, fructose, maltose, ABA, IAA)	YES (IAA, malic acid, citric acid, succinic acid, ABA, JA)
Electrode technology	LIG	Graphene coated with CuMOF	MWCNTs/Nafion modified carbon tape	CuMOF-carbon black-Nafion	Nitrogen-doped graphene	PtNf/ERGO/Pt
Abiotic or biotic stress monitoring	YES (drought and salinity)	YES (drought)	YES (pathogen)	YES (drought)	NO	YES (Salinity)
Portable sensor	YES	YES	YES	YES	YES	YES

CA: chronoamperometry, DPV: differential pulse voltammetry, ABA: abscisic acid, CuMOF: copper-based metal-organic framework, MWCNYs: multi-walled carbon nanotubes, GA: gibberellic acid, OA: oleic acid, IAA: indole-3-acetic acid.

The wearable biosensor designed for salicylic acid monitoring, based on LIG electrodes, operates on the principle of the electro-oxidative reaction of SA at an oxidation potential of 0.8 V. It boasts an impressive sensitivity of 82.3 nA/(μmol L^{-1}·cm^2) (equivalent to 14.83 nA/μmol L^{-1}) and a limit of detection of 8.2 μmol L^{-1}. When compared with the most relevant SA biosensor for plants available in the state of the art[222], it demonstrates a sensitivity improvement of over 99%. While it has a lower LOD, the linearity of the proposed sensor is 90% better than that demonstrated by the other work[222], especially within the SA concentration range of 1 – 1000 μmol L^{-1}. Moreover, this bio-agent-free technology exhibits outstanding selectivity, with minimal interference effects from common metabolites typically found in iontophoretic samples extracted from plant leaves, including sucrose, fructose, citric acid, and oxalic acid. The recent interest in developing SA biosensors for plants, as evidenced in Table 8, highlights the significance of this work. Among the various technologies listed, our developed sensor emerges as a highly competitive option, offering advantages such as non-invasive and real-time evaluation, portability, impressive sensitivity, and high linearity. Notably, only one additional study has reported on the non-invasive detection of SA in plants, as indicated in Table 8.

Considering the current advancements in sensing technologies for plants, as reflected in Table 6 and Table 7, the proposed technology represents a significant step forward in understanding the real-time dynamics of crucial plant metabolites and their relationship with stress tolerance responses. By investigating how plants differentiate the induction of phytohormones like SA and sugars such as glucose under different stress conditions, we can enhance the understanding of the specificities of plant responses to both biotic and abiotic stresses. This knowledge can also contribute to improving existing crop breeding strategies by enabling high-resolution phenotyping.

Furthermore, the proposed technologies exhibit significant potential for commercial viability, primarily owing to their cost-effective fabrication requirements for mass-producing electrodes using screen-printing and laser-induced techniques. Their portability and user-friendliness eliminate the need for highly trained personnel and specialized equipment, thereby reducing costs and making them even more attractive for widespread adoption.

Limitations of the Designed Biosensors

SARS-CoV-2 Biosensor

While the sensor demonstrated a coefficient of variance of 4.446%, it is important to address issues arising from the manual bio-modification of the SPCEs, as this can impact the overall repeatability of the sensor. These issues can be mitigated by employing finer-grain carbon-based paste for the SPCE thick-film screen printing process. Additionally, automation using a pipetting robot or a liquid-handling station, equipped with a Peltier-controlled SPCE sheet holder at 5°C and a multiplexed potentiostat configuration, can streamline surface functionalization and characterization protocols. To enhance linearity for virus concentrations exceeding 20 fg mL^{-1}, it may be beneficial to focus on optimizing antibody orientation. This enhancement can improve epitope binding, resulting in a stronger signal response at higher concentrations and greater sensor sensitivity. Furthermore, preserving the SPCEs in a controlled humid environment, including safeguarding the reference electrode in a saturated KCl solution, can reduce degradation caused by oxidation, contamination, and denaturing of bio-functional layers. While SPCE characteristics have been confirmed to remain consistent for up to one week, this can be further improved under controlled environments.

Glucose Biosensor

Thanks to the enzymatic mechanism used for glucose detection, the sensor achieved a coefficient of variance of 2.87%. However, there are certain limitations to consider. The PET substrate utilized for electrode fabrication lacks elasticity, limiting the stretchability of the electrode. Given that this sensor is intended for use in uncontrolled environments and on plants, external factors like climate can influence leaf morphology, directly impacting electrode response, repeatability, and stability. To address this issue, exploring alternative substrate materials such as paper-based and elastomeric materials could significantly improve the sensor's stretchability. Another challenge arises from enzymatic degradation, which restricts the sensor's lifespan due to the controlled environmental conditions required by the enzyme to prevent denaturation. Consequently, the fabricated electrode was designed as single-use, but this approach could raise concerns regarding the environmental impact, especially in large-scale agricultural applications. Therefore, investigating novel methods for selectively detecting glucose emerges as an environmentally responsible choice, potentially enhancing the commercial viability of this technology. Additionally, the use of solid magnets to attach the sensor to leaves can limit the device's form factor. Research into flexible magnets and alternative attachment methods is necessary to enhance the sensor's size and adaptability.

Salicylic Acid Biosensor

Fabrication parameters such as power and speed can directly influence the stability of LIG electrodes. Therefore, it is necessary to determine the most suitable values depending on the desired application. Although the SA biosensor exhibits a coefficient of variance of 8.2%, allowing for accurate and repeatable analyte concentration determination, this value can be further improved by optimizing the parameters of LIG fabrication for this specific application. Similarly, in the case of the glucose sensor, the electrode substrate, polyimide in this instance, limits the sensor's stretchability but offers high thermal tolerance, making it suitable for LIG fabrication. However, exploring new materials with higher elastic coefficients can enhance the electrode's adaptability to different leaf morphologies. Additionally, despite improvements in sensor reusability through the cleaning protocol involving NaOH, it is not recommended to use a single electrode more than 10 times for measurements. This is because the washing process can flake off graphene, potentially altering the electrode's surface and affecting stability, sensitivity, and reusability. Another noteworthy limitation to consider is the susceptibility of LIG electrodes to environmental factors such as humidity and temperature variations. These can introduce variability in sensor performance, especially in outdoor settings where climate conditions can be unpredictable. For this reason, the need for careful handling and storage to prevent contamination or physical damage to the fragile LIG electrodes can be a practical limitation in uncontrolled environments.

Future Work

Future work should primarily focus on further improving the biosensor technologies presented in this dissertation. Enhancements may include:

1. Automated fabrication and bio-modification processes to streamline production and increase efficiency.
2. Integration of microfluidic techniques to enhance the functionality and performance of the biosensors.
3. Exploration of new materials that offer increased flexibility and long-term stability for improved sensor performance.
4. Integration of the iontophoretic system onto the developed device (SenSARS) to enable diagnosis and analyte measurement from human sweat. This integration holds the potential to broaden the spectrum of detectable analytes, including but not limited to glucose, lactose, ketones, and more, thus expanding the range of applications and the capabilities of the device.
5. Integration of multiple sensors for environmental and physical monitoring of plant variables such as humidity, temperature, and water availability.

In addition to these improvements, there are specific challenges that need to be addressed in future research. These include:

1. Adapting the proposed leaf biosensor design for integration into a lab-on-chip device. This entails the microfabrication of all electronic circuitry, necessitating the creation of intricate patterns using materials like silicon, glass, or polymers to construct channels, electrodes, and other essential components. Additionally, there's a need to explore new power supply methods to reduce the overall size to a few square centimeters. Given that the sensor will be placed outdoors on the leaf, the incorporation of solar cells as power sources emerges as a noteworthy alternative. Furthermore, the fabrication of controlled microfluidic channels using microcontact printing techniques is essential to facilitate sample preparation, cleaning, and separation of samples obtained from the leaf. It's important to consider a microfluidic channel for transporting the extracted fluid from the leaf through reverse iontophoresis directly to the sensing area. Novel strategies for attaching the

sensor to the leaf must be explored. While flexible magnets may enhance leaf attachment, new methods to adapt the sensor to different leaf morphologies are needed. Moreover, the inclusion of a wireless communication system is imperative to transmit measured data to a computer or a mobile app. Given the expected low power consumption of the device, the Bluetooth Low Energy (BLE) protocol stands out as an attractive alternative. The purpose of creating such a compact device, as described here, is to reduce fabrication costs and size, thereby offering an attractive commercial system capable of real-time plant status monitoring. This, in turn, can facilitate the development of more effective control strategies to enhance agricultural production.

2. Conducting studies on the application of iontophoresis to plant leaves to comprehensively characterize its potential for non-invasively extracting plant samples. In this dissertation, all measurements were consistently performed on the same leaf of each plant species studied. This approach was adopted to minimize undesired variability in the resulting measurements. However, it is crucial to explore how measurements can vary from leaf to leaf, depending on specific characteristics such as distance from the stem, height with respect to roots, age, and degree of exposure to the environment. To achieve this, techniques such as High-Performance Liquid Chromatography (HPLC) or spectroscopy could provide valuable insights related to the quantification of the analyte of interest from different leaves on the same plant with varying characteristics. It is important to consider that plants undergo different biological processes throughout the day. Therefore, it is necessary to monitor the analyte of interest in short time intervals (< 4 hours) over a 24-hour period. Additionally, it will be indispensable to study the long-term impact that the application of reverse iontophoresis has on the plant's overall health and to quantify the number of measurements possible before affecting leaf integrity. Performing this analysis on at least three different plant species will provide sufficient information to determine the optimal points for monitoring the analyte of interest based on plant physiology. It is essential to note that there is currently limited information in the existing literature regarding the optimization of reverse iontophoresis for ensuring the optimal extraction of plant metabolites of interest. Therefore, this study has the potential to pioneer the development of the most suitable protocols for applying reverse iontophoresis to non-invasively extract plant samples.

3. Simultaneously performing *in-vivo*, *in-situ* and real-time detection of essential analytes such as salicylic acid (SA), ethylene (ET), jasmonic acid (JA) and abscisic acid (ABA),

could provide valuable insights in how different hormones crosstalk and interact in response to stressful environments in plants. For example, there is growing evidence that salicylic acid and jasmonic acid crosstalk to modulate the plant defenses against pathogen attacks. However, quantifying the precise contribution of each hormone to this process remains limited. To achieve simultaneous monitoring of at least four different hormones, a multiplexed electrochemical biosensor based on a microarray arrangement can be designed. In this setup, each spot on the array contains capture molecules on a microelectrode surface that specifically bind to a particular analyte. Fabricating closely spaced microelectrodes requires applying a pattern to a substrate using photolithography. Electrical connections for each microelectrode can then be established using metal leads or bonding wires. This approach creates a multisensory system capable of monitoring various compounds simultaneously in the reverse iontophoretic extract from plant leaves. Additionally, it is crucial to develop software for data integration and analysis. This software could rely on real-time signal processing blocks to filter noise and employ neural networks to merge data from each microelectrode, characterizing specific plant hormone behavior and interactions under distinct stress scenarios. Different stressors induce varying responses in plant hormone levels. For instance, elevated levels of certain phytohormones like ABA may indicate water stress, while increased SA levels might signal the presence of pathogens. Real-time monitoring of these analytes could enable the detection of individual or combined stress conditions before visible symptoms manifest, facilitating timely interventions and improving plant health management.

Conclusions

In this dissertation, the primary focus was on the development of non-invasive biosensor platforms for quantifying metabolites associated with human health and plant stress responses. The research aimed to address various challenges and limitations in the field of biosensors, particularly in terms of non-invasive extraction of plant metabolites and the selective and sensitive detection of target analytes in complex matrices. The dissertation presents several significant achievements:

1. To address the urgent need for rapid and accurate detection of SARS-CoV-2, the virus responsible for the COVID-19 pandemic, an electrochemical low-cost and portable POC device was developed. The device exhibited remarkable performance in terms of LOD (1 fg mL^{-1}) and specificity (>90%). Notably, these properties demonstrated remarkable improvements in LOD of more than 23% compared to traditional RT-PCR methods and an astonishing 99.98% enhancement over the most pertinent biosensor technology presented in the current state of the art. Furthermore, in terms of diagnostic time, this proposed technology reduces the diagnosis time to a mere 10 minutes, marking an impressive 91.67% improvement compared to the time-consuming RT-PCR method and a commendable 33.33% reduction compared to similar approaches. These significant reductions underscore the device's potential for efficient and early diagnosis of SARS-CoV-2 infections. In addition to its remarkable diagnostic capabilities, this technology exhibits scalability, and the potential for mass production, making it well-suited for global market introduction. Furthermore, its adaptability allows for seamless reconfiguration to detect other viruses or biomarkers by adjusting the sensor's selectivity and evaluation methods. Consequently, this versatile platform is expected to set the standard for the development of future low-cost diagnostic devices, promising a brighter future for efficient and accessible healthcare solutions.
2. A wearable biosensor was developed to enable real-time monitoring of glucose levels in plants, offering an *in-situ*, *in-vivo*, non-invasive, and non-destructive approach. The integration of an iontophoretic system facilitated rapid (<10 minutes) and clean sample extraction. Two magnetic holders were incorporated to ensure the easy positioning and removal of the sensor on leaves while protecting the sensing area from environmental exposure. This sensor demonstrated a limit of detection of 9.4 µmol L^{-1} and a sensitivity of 1.6 nA/µmol L^{-1}, marking remarkable improvements of over 130.98% and 99.95%,

respectively, compared to a relevant microneedle-based biosensor designed for *in-vivo* glucose monitoring in plants previously published in the state of the art. Furthermore, the device's sensing performance was assessed by monitoring glucose concentrations in three different plant species subjected to variations in light and temperature. These results provided quantitative insights into the behavior of this sugar under diverse environmental conditions, a novel contribution in plant science. Given that plant fluids contain a rich array of primary and secondary metabolites, the proposed sensor concept can be readily adapted to monitor other analytes of interest by adjusting the selectivity of the working electrode, as was demonstrated in the determination of salicylic acid.

3. To detect salicylic acid, a crucial signaling molecule in plants involved in defense against pathogens and abiotic stresses, a bioagent-free LIG electrode was adapted onto the developed wearable iontophoretic-based platform. This technology enables real-time, non-invasive monitoring of SA in plant leaves, offering notable advantages, including a sensitivity of 82.3 nA/ µmol L^{-1}·cm^{-2} and a LOD of 8.2 µmol L^{-1}. In terms of sensitivity and linearity, the proposed sensor demonstrated remarkable improvements of over 99% and 90%, respectively, compared to the first non-invasive biosensor presented in the state of the art for this analyte. Furthermore, the results highlighted the significant role of salicylic acid as a regulatory phytohormone in the adaptive responses of avocado plants to drought and salinity stresses. These findings unveiled distinct dynamics in SA accumulation, with drought stress inducing a rapid and substantial increase in SA levels, while salinity stress triggered a more gradual response. This research contributes valuable insights into plant stress responses and their potential applications in crop management and stress tolerance breeding programs.

References

1. Giraldo, J. P., Wu, H., Newkirk, G. M. & Kruss, S. Nanobiotechnology approaches for engineering smart plant sensors. *Nat Nanotechnol* **14**, 541–553 (2019).

2. Lee, G., Wei, Q. & Zhu, Y. Emerging Wearable Sensors for Plant Health Monitoring. *Adv Funct Mater* **31**, 1–14 (2021).

3. Perdomo, S. A., Marmolejo-Tejada, J. M. & Jaramillo-Botero, A. Review—Bio-Nanosensors: Fundamentals and Recent Applications. *J Electrochem Soc* **168**, 107506 (2021).

4. Jones, W. P. & Kinghorn, A. D. Extraction of Plant Secondary Metabolites. in *Methods in Molecular Biology* vol. 864 341–366 (Humana Press, 2012).

5. Kim, J., Campbell, A. S., de Ávila, B. E.-F. & Wang, J. Wearable biosensors for healthcare monitoring. *Nat Biotechnol* **37**, 389–406 (2019).

6. Ye, S., Feng, S., Huang, L. & Bian, S. Recent Progress in Wearable Biosensors: From Healthcare Monitoring to Sports Analytics. *Biosensors (Basel)* **10**, 1–34 (2020).

7. Xu, J., Fang, Y. & Chen, J. Wearable Biosensors for Non-Invasive Sweat Diagnostics. *Biosensors (Basel)* **11**, 1–21 (2021).

8. Lin, Y., Bariya, M. & Javey, A. Wearable Biosensors for Body Computing. *Adv Funct Mater* **31**, 2008087 (2021).

9. De la Paz, E. *et al.* Extended Noninvasive Glucose Monitoring in the Interstitial Fluid Using an Epidermal Biosensing Patch. *Anal Chem* **93**, 12767–12775 (2021).

10. De la Paz, E. *et al.* Non-invasive monitoring of interstitial fluid lactate through an epidermal iontophoretic device. *Talanta* **254**, 124122 (2023).

11. Moon, J. M. *et al.* Self-Testing of Ketone Bodies, along with Glucose, Using Touch-Based Sweat Analysis. *ACS Sens* **7**, 3973–3981 (2022).

12. Nidzworski, D. *et al.* A rapid-response ultrasensitive biosensor for influenza virus detection using antibody modified boron-doped diamond. *Sci Rep* **7**, 15707 (2017).

13. Kim, H. E. *et al.* Sensitive electrochemical biosensor combined with isothermal amplification for point-of-care COVID-19 tests. *Biosens Bioelectron* **182**, 113168 (2021).

14. Nandi, S., Mondal, A., Roberts, A. & Gandhi, S. Biosensor platforms for rapid HIV detection. *Adv Clin Chem* **98**, 1–34 (2020).

15. Chen, Y. *et al.* Field-Effect Transistor Biosensor for Rapid Detection of Ebola Antigen. *Scientific Reports 2017 7:1* **7**, 1–8 (2017).

16. Kim, J., Campbell, A. S., de Ávila, B. E. F. & Wang, J. Wearable biosensors for healthcare monitoring. *Nature Biotechnology 2019 37:4* **37**, 389–406 (2019).

17. Barbosa, J. A. *et al.* Biocompatible Wearable Electrodes on Leaves toward the On-Site Monitoring of Water Loss from Plants. *ACS Appl Mater Interfaces* **14**, 22989–23001 (2022).

18. Desagani, D., Jog, A., Teig-Sussholz, O., Avni, A. & Shacham-Diamand, Y. Drought monitoring in tobacco plants by in-vivo electrochemical biosensor. *Sens Actuators B Chem* **356**, 131357 (2022).

19. Conesa, M. R., Conejero, W., Vera, J. & Ruiz-Sánchez, M. C. Assessment of trunk microtensiometer as a novel biosensor to continuously monitor plant water status in nectarine trees. *Front Plant Sci* **14**, 1123045 (2023).

20. Rathnayake, I. V. N., Megharaj, M. & Naidu, R. Green fluorescent protein based whole cell bacterial biosensor for the detection of bioavailable heavy metals in soil environment. *Environ Technol Innov* **23**, 101785 (2021).

21. Abbas, S. Z. *et al.* Recent advances in soil microbial fuel cells based self-powered biosensor. *Chemosphere* **303**, 135036 (2022).

22. Camila Ayala, M., Lorena López, L., Jaramillo-Botero, A. & Valencia, D. Electrochemical modified electrode with bismuth film for ultrasensitive determination of aluminum (iii). *Journal of Electroanalytical Chemistry* **919**, 116552 (2022).

23. Ma, Z. *et al.* A Fast and Easily Parallelizable Biosensor Method for Measuring Extractable Tetracyclines in Soils. *Environ Sci Technol* **54**, 758–767 (2020).

24. Lu, Y. *et al.* Multimodal Plant Healthcare Flexible Sensor System. *ACS Nano* **14**, 10966–10975 (2020).

25. Nassar, J. M. *et al.* Compliant plant wearables for localized microclimate and plant growth monitoring. *npj Flex Electron* **2**, 24 (2018).

26. Zhao, Y. *et al.* Multifunctional Stretchable Sensors for Continuous Monitoring of Long-Term Leaf Physiology and Microclimate. *ACS Omega* **4**, 9522–9530 (2019).

27. Lee, G. *et al.* Abaxial leaf surface-mounted multimodal wearable sensor for continuous plant physiology monitoring. *Sci Adv* **9**, eade2232 (2023).

28. Dong, K. *et al.* Flexible and Shape-Morphing Plant Sensors Designed for Microenvironment Temperature Monitoring of Irregular Surfaces. *Adv Mater Technol* **8**, 2201204 (2023).

29. Zheng, C., Zhou, Q., Wang, J. & Du, D. Wireless plant stresses monitoring with a wearable chemiresistor gas sensor at room temperature. *Sens Actuators B Chem* **381**, 133408 (2023).

30. Patel, R. *et al.* Part I: Non-faradaic electrochemical impedance-based DNA biosensor for detecting phytopathogen – Ralstonia solanacearum. *Bioelectrochemistry* **150**, 108370 (2023).

31. Tameh, M. H. *et al.* Pectobacterium atrosepticum Biosensor for Monitoring Blackleg and Soft Rot Disease of Potato. *Biosensors 2020, Vol. 10, Page 64* **10**, 64 (2020).

32. Luna-Moreno, D. *et al.* Early Detection of the Fungal Banana Black Sigatoka Pathogen Pseudocercospora fijiensis by an SPR Immunosensor Method. *Sensors 2019, Vol. 19, Page 465* **19**, 465 (2019).

33. Cebula, Z. *et al.* Detection of the Plant Pathogen Pseudomonas Syringae pv. Lachrymans on Antibody-Modified Gold Electrodes by Electrochemical Impedance Spectroscopy. *Sensors 2019, Vol. 19, Page 5411* **19**, 5411 (2019).

34. Lei, R. *et al.* Ultrasensitive isothermal detection of a plant pathogen by using a gold nanoparticle-enhanced microcantilever sensor. *Sens Actuators B Chem* **338**, 129874 (2021).

35. Veltman, B. *et al.* Whole-cell bacterial biosensor for volatile detection from Pectobacterium-infected potatoes enables early identification of potato tuber soft rot disease. *Talanta* **247**, 123545 (2022).

36. Ma, W. *et al.* An odorant receptor-derived peptide biosensor for monitoring the occurrence of Hyphantria cunea larvae by recognizing herbivore-induced plant volatile. *Sens Actuators B Chem* **381**, 133432 (2023).

37. Yan, X. *et al.* Flexible Aggregation-Induced Emission-Active Hydrogel for On-Site Monitoring of Pesticide Degradation. *ACS Nano* **16**, 18421–18429 (2022).

38. Wang, D. *et al.* Dual-functional ultrathin wearable 3D particle-in-cavity SF-AAO-Au SERS sensors for effective sweat glucose and lab-on-glove pesticide detection. *Sens Actuators B Chem* **359**, 131512 (2022).

39. Zhao, F. *et al.* Smart plant-wearable biosensor for in-situ pesticide analysis. *Biosens Bioelectron* **170**, 112636 (2020).

40. Wu, Z. *et al.* Near-infrared-excitable acetylcholinesterase-activated fluorescent probe for sensitive and anti-interference detection of pesticides in colored food. *Biosens Bioelectron* **233**, 115341 (2023).

41. Bao, J. *et al.* Plant Esterase-Chitosan/Gold Nanoparticles-Graphene Nanosheet Composite-Based Biosensor for the Ultrasensitive Detection of Organophosphate Pesticides. *J Agric Food Chem* **63**, 10319–10326 (2015).

42. Diacci, C. *et al.* Diurnal in vivo xylem sap glucose and sucrose monitoring using implantable organic electrochemical transistor sensors. *iScience* **24**, 101966 (2021).

43. Ruiz-Gonzalez, A., Kempson, H. & Haseloff, J. A Simple Reversed Iontophoresis-Based Sensor to Enable In Vivo Multiplexed Measurement of Plant Biomarkers Using Screen-Printed Electrodes. *Sensors* **23**, 780 (2023).

44. Ishtiaque Hossain, N. & Tabassum, S. Stem-FIT: a Microneedle-based Multi-parametric Sensor for In Situ Monitoring of Salicylic Acid and pH Levels in Live Plants. *17th IEEE International Conference on Nano/Micro Engineered and Molecular Systems, NEMS 2022* 312–316 (2022) doi:10.1109/NEMS54180.2022.9791212.

45. Bukhamsin, A. *et al.* Minimally-invasive, real-time, non-destructive, species-independent phytohormone biosensor for precision farming. *Biosens Bioelectron* **214**, 114515 (2022).

46. Fan, C. X. *et al.* All-solid-state potentiometric salicylic acid sensor for in-situ measurement of plant. *Anal Bioanal Chem* **415**, 1979–1989 (2023).

47. Chen, C. *et al.* Development of a structure-switching aptamer-based nanosensor for salicylic acid detection. *Biosens Bioelectron* **140**, 111342 (2019).

48. Detpisuttitham, W., Phanthong, C., Ngamchana, S., Rijiravanich, P. & Surareungchai, W. Electrochemical Detection of Salicylic Acid in Pickled Fruit/Vegetable and Juice. *J Anal Test* **4**, 291–297 (2020).

49. Sun, L. J. *et al.* Paper-based electroanalytical devices for in situ determination of salicylic acid in living tomato leaves. *Biosens Bioelectron* **60**, 154–160 (2014).

50. Zhang, W. De *et al.* Electrochemical oxidation of salicylic acid at well-aligned multiwalled carbon nanotube electrode and its detection. *Journal of Solid State Electrochemistry* **14**, 1713–1718 (2010).

51. Li, M. *et al.* Development of a simple disposable laser-induced porous graphene flexible electrode for portable wireless intelligent votammetric nanosensing of salicylic acid in agro-products. *Comput Electron Agric* **191**, 106502 (2021).

52. Zhang, F. *et al.* Fabrication of self-supporting nitrogen-doped graphene microelectrodes for in situ analysis of salicylic acid in plants. *Carbon N Y* **175**, 364–376 (2021).

53. Hu, Y. *et al.* In vivo detection of salicylic acid in sunflower seedlings under salt stress. *RSC Adv* **8**, 23404–23410 (2018).

54. Sneha, M., Ravindranath, N. A., Murugesan, N. & Jayaraman, V. A biosensor for monitoring of salt stress in plants. *Org Electron* **113**, 106698 (2023).

55. Ruiz-gonzalez, A., Kempson, H. & Haseloff, J. In Vivo Sensing of pH in Tomato Plants Using a Low-Cost and Open-Source Device for Precision Agriculture. *Biosensors 2022, Vol. 12, Page 447* **12**, 447 (2022).

56. *Sustainable Agriculture, Forest and Environmental Management*. *Sustainable Agriculture, Forest and Environmental Management* (Springer Singapore, 2019). doi:10.1007/978-981-13-6830-1.

57. Arora, N. K. Impact of climate change on agriculture production and its sustainable solutions. *Environmental Sustainability* **2**, 95–96 (2019).

58. Sharma, S., Kooner, R. & Arora, R. Insect Pests and Crop Losses. in *Breeding Insect Resistant Crops for Sustainable Agriculture* 45–66 (Springer Singapore, 2017). doi:10.1007/978-981-10-6056-4_2.

59. Salehi-Lisar, S. Y. & Bakhshayeshan-Agdam, H. Drought Stress in Plants: Causes, Consequences, and Tolerance. in *Drought Stress Tolerance in Plants, Vol 1* 1–16 (Springer International Publishing, 2016). doi:10.1007/978-3-319-28899-4_1.

60. Farooq, M., Hussain, M., Wahid, A. & Siddique, K. H. M. Drought Stress in Plants: An Overview. in *Plant Responses to Drought Stress* vol. 9783642326530 1–33 (Springer Berlin Heidelberg, 2012).

61. Hassan, M. U. *et al.* Heat stress in cultivated plants: nature, impact, mechanisms, and mitigation strategies—a review. *Plant Biosystems - An International Journal Dealing with all Aspects of Plant Biology* **155**, 211–234 (2021).

62. Thakur, P., Kumar, S., Malik, J. A., Berger, J. D. & Nayyar, H. Cold stress effects on reproductive development in grain crops: An overview. *Environ Exp Bot* **67**, 429–443 (2010).

63. Isayenkov, S. V. & Maathuis, F. J. M. Plant Salinity Stress: Many Unanswered Questions Remain. *Front Plant Sci* **10**, 1–11 (2019).

64. Tewari, S. & Mishra, A. Flooding Stress in Plants and Approaches to Overcome. in *Plant Metabolites and Regulation Under Environmental Stress* 355–366 (Elsevier, 2018). doi:10.1016/B978-0-12-812689-9.00018-2.

65. Yang, B. *et al.* Light Stress Responses and Prospects for Engineering Light Stress Tolerance in Crop Plants. *J Plant Growth Regul* **38**, 1489–1506 (2019).

66. Singh, J. & Thakur, J. K. Photosynthesis and Abiotic Stress in Plants. in *Biotic and Abiotic Stress Tolerance in Plants* 27–46 (Springer Singapore, 2018). doi:10.1007/978-981-10-9029-5_2.

67. Ghori, N.-H. *et al.* Heavy metal stress and responses in plants. *Int. J. Environ. Sci. Technol.* **16**, 1807–1828 (2019).

68. Forzato, C., Vida, V. & Berti, F. Biosensors and Sensing Systems for Rapid Analysis of Phenolic Compounds from Plants: A Comprehensive Review. *Biosensors (Basel)* **10**, 105 (2020).

69. Li, Z., Zhou, J., Dong, T., Xu, Y. & Shang, Y. Application of electrochemical methods for the detection of abiotic stress biomarkers in plants. *Biosens Bioelectron* **182**, 113105 (2021).

70. Liu, J. Smart-agriculture: wearable devices for plant protection. in *Wearable Physical, Chemical and Biological Sensors* 275–294 (Elsevier, 2022). doi:10.1016/B978-0-12-821661-3.00002-1.

71. Qu, C. *et al.* Flexible Wearables for Plants. *Small* **17**, 2104482 (2021).

72. Jaramillo-Botero, A. *et al.* The ÓMICAS alliance, an international research program on multi-omics for crop breeding optimization. *Front Plant Sci* **13**, 1–20 (2022).

73. Li, Y. *et al.* Plant-Wearable Sensors for Intelligent Forestry Monitoring. *Adv Sustain Syst* **7**, 2200333 (2023).

74. Perumal, V. & Hashim, U. Advances in biosensors: Principle, architecture and applications. *J Appl Biomed* **12**, 1–15 (2014).

75. Kumar, S. & Kalkal, A. Electrochemical detection: Cyclic voltammetry/differential pulse voltammetry/impedance spectroscopy. in *Nanotechnology in Cancer Management* (eds. Khondakar, K. R. & Kaushik, A. K.) 43–71 (Elsevier, 2021). doi:10.1016/B978-0-12-818154-6.00008-1.

76. Zhang, K., Lv, S., Zhou, Q. & Tang, D. CoOOH nanosheets-coated g-C3N4/CuInS2 nanohybrids for photoelectrochemical biosensor of carcinoembryonic antigen coupling hybridization chain reaction with etching reaction. *Sens Actuators B Chem* **307**, 127631 (2020).

77. Zeng, R. *et al.* Palindromic Molecular Beacon Based Z-Scheme BiOCl-Au-CdS Photoelectrochemical Biodetection. *Anal Chem* **91**, 2447–2454 (2019).

78. Zhang, B., Liu, B., Chen, G. & Tang, D. Competitive-type displacement reaction for direct potentiometric detection of low-abundance protein. *Biosens Bioelectron* **53**, 465–471 (2014).

79. Lv, S., Lin, Z., Zhang, K., Lu, M. & Tang, D. Polyion oligonucleotide-decorated gold nanoparticles with tunable surface charge density for amplified signal output of potentiometric immunosensor. *Anal Chim Acta* **964**, 67–73 (2017).

80. Zdrachek, E. & Bakker, E. Potentiometric Sensing. *Anal Chem* **91**, 2–26 (2019).

81. Hu, J., Stein, A. & Bühlmann, P. Rational design of all-solid-state ion-selective electrodes and reference electrodes. *TrAC Trends in Analytical Chemistry* **76**, 102–114 (2016).

82. Chou, J.-C. *et al.* A Sensitive Potentiometric Biosensor Using MBs-AO/GO/ZnO Membranes-Based Arrayed Screen-Printed Electrodes for AA Detection and Remote Monitoring. *IEEE Access* **7**, 105962–105972 (2019).

83. Silva, N. F. D. *et al.* Development of a disposable paper-based potentiometric immunosensor for real-time detection of a foodborne pathogen. *Biosens Bioelectron* **141**, 111317 (2019).

84. Deng, K., Zhang, Y. & Tong, X.-D. A novel potentiometric immunoassay for carcinoma antigen 15-3 by coupling enzymatic biocatalytic precipitation with a nanogold labelling strategy. *Analyst* **143**, 1454–1461 (2018).

85. Han, T., Mattinen, U. & Bobacka, J. Improving the Sensitivity of Solid-Contact Ion-Selective Electrodes by Using Coulometric Signal Transduction. *ACS Sens* **4**, 900–906 (2019).

86. Scholz, F. Voltammetric techniques of analysis: the essentials. *ChemTexts* **1**, 17 (2015).

87. Batchelor-McAuley, C. *et al.* Recent Advances in Voltammetry. *ChemistryOpen* **4**, 224–260 (2015).

88. Elgrishi, N. *et al.* A Practical Beginner's Guide to Cyclic Voltammetry. *J Chem Educ* **95**, 197–206 (2018).

89. Li, L. *et al.* Aptamer based voltammetric biosensor for Mycobacterium tuberculosis antigen ESAT-6 using a nanohybrid material composed of reduced graphene oxide and a metal-organic framework. *Microchimica Acta* **185**, 379 (2018).

90. Li, W., Shu, D., Zhang, D. & Ma, Z. Multi-amplification of the signal of voltammetric immunosensors: Highly sensitive detection of tumor marker. *Sens Actuators B Chem* **262**, 50–56 (2018).

91. Vieira Thomaz, D. Development of Laccase-TiO2@Carbon Paste Biosensor for Voltammetric Determination of Paracetamol. *Int J Electrochem Sci* **13**, 10884–10893 (2018).

92. Bollella, P. & Gorton, L. Enzyme based amperometric biosensors. *Curr Opin Electrochem* **10**, 157–173 (2018).

93. Cordeiro, C. A., Sias, A., Koster, T., Westerink, B. H. C. & Cremers, T. I. F. H. In vivo “real-time” monitoring of glucose in the brain with an amperometric enzyme-based biosensor based on gold coated tungsten (W-Au) microelectrodes. *Sens Actuators B Chem* **263**, 605–613 (2018).

94. Li, L. *et al.* All Inkjet-Printed Amperometric Multiplexed Biosensors Based on Nanostructured Conductive Hydrogel Electrodes. *Nano Lett* **18**, 3322–3327 (2018).

95. Kucherenko, D. Yu. *et al.* A highly selective amperometric biosensor array for the simultaneous determination of glutamate, glucose, choline, acetylcholine, lactate and pyruvate. *Bioelectrochemistry* **128**, 100–108 (2019).

96. Guerrieri, A., Ciriello, R., Crispo, F. & Bianco, G. Detection of choline in biological fluids from patients on haemodialysis by an amperometric biosensor based on a novel anti-interference bilayer. *Bioelectrochemistry* **129**, 135–143 (2019).

97. Jiang, B., Dong, P. & Zheng, J. A novel amperometric biosensor based on covalently attached multilayer assemblies of gold nanoparticles, diazo-resins and acetylcholinesterase for the detection of organophosphorus pesticides. *Talanta* **183**, 114–121 (2018).

98. Perera, G. S. *et al.* Rapid and Selective Biomarker Detection with Conductometric Sensors. *Small* **17**, 1–12 (2021).

99. Bhardwaj, S. K. *et al.* TCNQ-doped Cu-metal organic framework as a novel conductometric immunosensing platform for the quantification of prostate cancer antigen. *Sens Actuators B Chem* **240**, 10–17 (2017).

100. Kolahchi, N. *et al.* Direct detection of phenol using a new bacterial strain-based conductometric biosensor. *J Environ Chem Eng* **6**, 478–484 (2018).

101. Bigdeli, I. K., Yeganeh, M., Shoushtari, M. T. & Zadeh, M. K. Electrochemical impedance spectroscopy (EIS) for biosensing. in *Nanosensors for Smart Manufacturing* (eds. Thomas, S., Nguyen, T. A., Ahmadi, M., Farmani, A. & Yasin, G.) 533–554 (Elsevier, 2021). doi:10.1016/B978-0-12-823358-0.00025-3.

102. Strong, M. E., Richards, J. R., Torres, M., Beck, C. M. & La Belle, J. T. Faradaic electrochemical impedance spectroscopy for enhanced analyte detection in diagnostics. *Biosens Bioelectron* **177**, 112949 (2021).

103. Chang, B.-Y. & Park, S.-M. Electrochemical Impedance Spectroscopy. *Annual Review of Analytical Chemistry* **3**, 207–229 (2010).

104. Sopoušek, J., Věžník, J., Houser, J., Skládal, P. & Lacina, K. Crucial factors governing the electrochemical impedance on protein-modified surfaces. *Electrochim Acta* **388**, (2021).

105. Bahner, N. *et al.* An aptamer-based biosensor for detection of doxorubicin by electrochemical impedance spectroscopy. *Anal Bioanal Chem* **410**, 1453–1462 (2018).

106. Elshafey, R. & Radi, A.-E. Electrochemical impedance sensor for herbicide alachlor based on imprinted polymer receptor. *Journal of Electroanalytical Chemistry* **813**, 171–177 (2018).

107. Ariño, C., Serrano, N., Díaz-Cruz, J. M. & Esteban, M. Voltammetric determination of metal ions beyond mercury electrodes. A review. *Anal Chim Acta* **990**, 11–53 (2017).

108. Cruz-Navarro, J. A., Hernandez-Garcia, F. & Alvarez Romero, G. A. Novel applications of metal-organic frameworks (MOFs) as redox-active materials for elaboration of carbon-based electrodes with electroanalytical uses. *Coord Chem Rev* **412**, 213263 (2020).

109. Russo, M. J. *et al.* Lubricin (PRG4) reduces fouling susceptibility and improves sensitivity of carbon-based electrodes. *Electrochim Acta* **333**, 135574 (2020).

110. Ryu, J. H. *et al.* All-carbon electrode consisting of carbon nanotubes on graphite foil for flexible electrochemical applications. *Materials* **7**, 1975–1983 (2014).

111. Chen, L., Tang, Y., Wang, K., Liu, C. & Luo, S. Direct electrodeposition of reduced graphene oxide on glassy carbon electrode and its electrochemical application. *Electrochem commun* **13**, 133–137 (2011).

112. Yi, Y. *et al.* Electrochemical corrosion of a glassy carbon electrode. *Catal Today* **295**, 32–40 (2017).

113. Macpherson, J. V. A practical guide to using boron doped diamond in electrochemical research. *Physical Chemistry Chemical Physics* **17**, 2935–2949 (2015).

114. Yang, N. *et al.* Conductive diamond: synthesis, properties, and electrochemical applications. *Chem Soc Rev* **48**, 157–204 (2019).

115. Sarakhman, O. & Švorc, Ľ. A Review on Recent Advances in the Applications of Boron-Doped Diamond Electrochemical Sensors in Food Analysis. *Crit Rev Anal Chem* 1–23 (2020) doi:10.1080/10408347.2020.1828028.

116. Li, H. *et al.* A novel modification to boron-doped diamond electrode for enhanced, selective detection of dopamine in human serum. *Carbon N Y* **171**, 16–28 (2021).

117. Allahverdiyeva, S. *et al.* Electroanalytical investigation and determination of hepatitis C antiviral drug ledipasvir at a non-modified boron-doped diamond electrode. *Diam Relat Mater* **108**, 107962 (2020).

118. Pereira, D. F., Santana, E. R., Piovesan, J. V. & Spinelli, A. A novel electrochemical strategy for determination of vitamin B12 by Co(I/II) redox pair monitoring with boron-doped diamond electrode. *Diam Relat Mater* **105**, 107793 (2020).

119. Almeida, C. M. V. B. & Giannetti, B. F. A new and practical carbon paste electrode for insoluble and ground samples. *Electrochem commun* **4**, 985–988 (2002).

120. Tajik, S. *et al.* Developments and applications of nanomaterial-based carbon paste electrodes. *RSC Adv* **10**, 21561–21581 (2020).

121. Antuña-Jiménez, D., González-García, M. B., Hernández-Santos, D. & Fanjul-Bolado, P. Screen-Printed Electrodes Modified with Metal Nanoparticles for Small Molecule Sensing. *Biosensors (Basel)* **10**, 9 (2020).

122. Barton, J. *et al.* Screen-printed electrodes for environmental monitoring of heavy metal ions: a review. *Microchimica Acta* **183**, 503–517 (2016).

123. Ahmed, M. U. *et al.* Toward the development of smart and low cost point-of-care biosensors based on screen printed electrodes. *Crit Rev Biotechnol* **36**, 1–11 (2015).

124. Mohamed, H. M. Screen-printed disposable electrodes: Pharmaceutical applications and recent developments. *TrAC Trends in Analytical Chemistry* **82**, 1–11 (2016).

125. Yao, B. *et al.* Paper-Based Electrodes for Flexible Energy Storage Devices. *Advanced Science* **4**, 1700107 (2017).

126. Preston, C. *et al.* Silver nanowire transparent conducting paper-based electrode with high optical haze. *J Mater Chem C Mater* **2**, 1248–1254 (2014).

127. Ronkainen, N. J., Halsall, H. B. & Heineman, W. R. Electrochemical biosensors. *Chem Soc Rev* **39**, 1747 (2010).

128. Zhu, Y.-C. *et al.* Enzyme-Based Biosensors and Their Applications. in *Advances in Enzyme Technology* 201–223 (Elsevier, 2019). doi:10.1016/B978-0-444-64114-4.00008-X.

129. Mohamad, N. R., Marzuki, N. H. C., Buang, N. A., Huyop, F. & Wahab, R. A. An overview of technologies for immobilization of enzymes and surface analysis techniques for immobilized enzymes. *Biotechnology & Biotechnological Equipment* **29**, 205–220 (2015).

130. Sirisha, V. L., Jain, A. & Jain, A. Enzyme Immobilization: An Overview on Methods, Support Material, and Applications of Immobilized Enzymes. in *Advances in Food and Nutrition Research* vol. 79 179–211 (Elsevier Inc., 2016).

131. Singh, A., Negi, M. S., Dubey, A., Kumar, V. & Verma, A. K. Methods of Enzyme Immobilization and Its Applications in Food Industry. in *Enzymes in Food Technology* 103–124 (Springer Singapore, 2018). doi:10.1007/978-981-13-1933-4_6.

132. Arugula, M. A. & Simonian, A. Novel trends in affinity biosensors: current challenges and perspectives. *Meas Sci Technol* **25**, 032001 (2014).

133. Leonardo, S., Toldrà, A. & Campàs, M. Biosensors based on isothermal DNA amplification for bacterial detection in food safety and environmentalmonitoring. *Sensors (Switzerland)* **21**, 1–24 (2021).

134. Rafique, B., Iqbal, M., Mehmood, T. & Shaheen, M. A. Electrochemical DNA biosensors: a review. *Sensor Review* **39**, 34–50 (2019).

135. Hashkavayi, A. B. & Raoof, J. B. Nucleic acid–based electrochemical biosensors. in *Electrochemical Biosensors* 253–276 (Elsevier, 2019). doi:10.1016/B978-0-12-816491-4.00009-7.

136. Ferapontova, E. E. DNA Electrochemistry and Electrochemical Sensors for Nucleic Acids. *Annual Review of Analytical Chemistry* **11**, 197–218 (2018).

137. Drobysh, M., Ramanaviciene, A., Viter, R. & Ramanavicius, A. Affinity Sensors for the Diagnosis of COVID-19. *Micromachines (Basel)* **12**, 390 (2021).

138. Lv, S., Zhang, K., Lin, Z. & Tang, D. Novel photoelectrochemical immunosensor for disease-related protein assisted by hemin/G-quadruplex-based DNAzyme on gold nanoparticles to enhance cathodic photocurrent on p-CuBi2O4 semiconductor. *Biosens Bioelectron* **96**, 317–323 (2017).

139. Lv, S. *et al.* H 2 -Based Electrochemical Biosensor with Pd Nanowires@ZIF-67 Molecular Sieve Bilayered Sensing Interface for Immunoassay. *Anal Chem* **91**, 12055–12062 (2019).

140. Cai, G., Yu, Z., Tong, P. & Tang, D. Ti 3 C 2 MXene quantum dot-encapsulated liposomes for photothermal immunoassays using a portable near-infrared imaging camera on a smartphone. *Nanoscale* **11**, 15659–15667 (2019).

141. Felix, F. S. & Angnes, L. Electrochemical immunosensors – A powerful tool for analytical applications. *Biosens Bioelectron* **102**, 470–478 (2018).

142. Hosu, O., Selvolini, G., Cristea, C. & Marrazza, G. Electrochemical Immunosensors for Disease Detection and Diagnosis. *Curr Med Chem* **25**, 4119–4137 (2018).

143. Mahato, K. *et al.* Electrochemical Immunosensors: Fundamentals and Applications in Clinical Diagnostics. in *Handbook of Immunoassay Technologies* 359–414 (Elsevier, 2018). doi:10.1016/B978-0-12-811762-0.00014-1.

144. Cotchim, S., Thavarungkul, P., Kanatharana, P. & Limbut, W. Multiplexed label-free electrochemical immunosensor for breast cancer precision medicine. *Anal Chim Acta* **1130**, 60–71 (2020).

145. Ku, S., Palanisamy, S. & Chen, S.-M. Highly selective dopamine electrochemical sensor based on electrochemically pretreated graphite and nafion composite modified screen printed carbon electrode. *J Colloid Interface Sci* **411**, 182–186 (2013).

146. El-Said, W. A., Abd El-Hameed, K., Abo El-Maali, N. & Sayyed, H. G. Label-free Electrochemical Sensor for Ex-vivo Monitoring of Alzheimer's Disease Biomarker. *Electroanalysis* **29**, 748–755 (2017).

147. Yola, M. L. & Atar, N. Novel voltammetric tumor necrosis factor-alpha (TNF-α) immunosensor based on gold nanoparticles involved in thiol-functionalized multi-walled carbon nanotubes and bimetallic Ni/Cu-MOFs. *Anal Bioanal Chem* **413**, 2481–2492 (2021).

148. Liv, L., Çoban, G., Nakiboğlu, N. & Kocagöz, T. A rapid, ultrasensitive voltammetric biosensor for determining SARS-CoV-2 spike protein in real samples. *Biosens Bioelectron* **192**, 113497 (2021).

149. Uludag, Y. & Köktürk, G. Determination of prostate-specific antigen in serum samples using gold nanoparticle based amplification and lab-on-a-chip based amperometric detection. *Microchimica Acta* **182**, 1685–1691 (2015).

150. Saeed, A. A., Sánchez, J. L. A., O'Sullivan, C. K. & Abbas, M. N. DNA biosensors based on gold nanoparticles-modified graphene oxide for the detection of breast cancer biomarkers for early diagnosis. *Bioelectrochemistry* **118**, 91–99 (2017).

151. Singal, S., Srivastava, A. K., Gahtori, B. & Rajesh. Immunoassay for troponin I using a glassy carbon electrode modified with a hybrid film consisting of graphene and multiwalled carbon nanotubes and decorated with platinum nanoparticles. *Microchimica Acta* **183**, 1375–1384 (2016).

152. Perdomo, S. *et al.* A Low-Cost Portable Electrochemical System for Ultra-sensitive, Near Real-time, Diagnostics of SARS-CoV-2 Infections. *Under Review in IEEE Transactions on Intrumentation and Measurement* (2021).

153. Liu, W. *et al.* Molecularly imprinted polymers on graphene oxide surface for EIS sensing of testosterone. *Biosens Bioelectron* **92**, 305–312 (2017).

154. Fidler, J. C., Penrose, W. R. & Bobis, J. P. A potentiostat based on a voltage-controlled current source for use with amperometric gas sensors. *IEEE Trans Instrum Meas* **41**, 308–310 (1992).

155. Gopinath, A. V. & Russell, D. An Inexpensive Field-Portable Programmable Potentiostat. *Chem. Educator* **6**, 1–6 (2005).

156. Blanco, J. R. *et al.* Design of a Low-Cost Portable Potentiostat for Amperometric Biosensors. in *2006 IEEE Instrumentation and Measurement Technology Conference Proceedings* 690–694 (IEEE, 2006). doi:10.1109/IMTC.2006.328670.

157. Moskovkin, O. V. A circuit for automatic compensation of the ohmic resistance of a solution in a three-electrode chemical cell by the current chopping method. *Instruments and Experimental Techniques* **43**, 403–405 (2000).

158. Hsu, C.-L., Zhang, T., Lo, Y.-H. & Hall, D. A. A low-noise gain-enhanced readout amplifier for induced molecular electronic signals. in *2015 IEEE Biomedical Circuits and Systems Conference (BioCAS)* 1–4 (IEEE, 2015). doi:10.1109/BioCAS.2015.7348407.

159. Ferrari, G., Gozzini, F. & Sampietro, M. Transimpedance Amplifiers for Extremely High Sensitivity Impedance Measurements on Nanodevices. in *Analog Circuit Design* 193–207 (Springer Netherlands, 2006). doi:10.1007/978-1-4020-8944-2_11.

160. Ferrari, G. & Sampietro, M. Wide bandwidth transimpedance amplifier for extremely high sensitivity continuous measurements. *Review of Scientific Instruments* **78**, 094703 (2007).

161. Dai, S. & Rosenstein, J. K. A dual-mode low-noise nanosensor front-end with 155-dB dynamic range. in *2015 IEEE Biomedical Circuits and Systems Conference (BioCAS)* 1–4 (IEEE, 2015). doi:10.1109/BioCAS.2015.7348404.

162. Bianchi, V. *et al.* A Wi-Fi Cloud-Based Portable Potentiostat for Electrochemical Biosensors. *IEEE Trans Instrum Meas* **69**, 3232–3240 (2020).

163. Pernia, A. M., Prieto, M. J., Orille, I. C., Martin-Ramos, J. A. & Costa-Garcia, A. Development of Optimized Screen-Printed Immunosensors. *IEEE Trans Instrum Meas* **58**, 2181–2188 (2009).

164. de la Roche, J., López-Cifuentes, I. & Jaramillo-Botero, A. Influence of lasing parameters on the morphology and electrical resistance of polyimide-based laser-induced graphene (LIG). *Carbon Letters* **33**, 587–595 (2023).

165. Park, J. & Eun, C. Electrochemical Behavior and Determination of Salicylic Acid at Carbon-fiber Electrodes. *Electrochim Acta* **194**, 346–356 (2016).

166. Lasia, A. Electrochemical Impedance Spectroscopy and its Applications. in *Modern Aspects of Electrochemistry* vol. 32 143–248 (Kluwer Academic Publishers, 2002).

167. Yang, C., Rairigh, D. & Mason, A. On-Chip Electrochemical Impedance Spectroscopy for Biosensor Arrays. in *2006 5th IEEE Conference on Sensors* 93–96 (IEEE, 2006). doi:10.1109/ICSENS.2007.355726.

168. Sánchez, M. I. G., McCullagh, J., Guy, R. H. & Compton, R. G. Reverse Iontophoretic Extraction of Metabolites from Living Plants and their Identification by Ion-chromatography Coupled to High Resolution Mass Spectrometry. *Phytochem Anal* **28**, 195–201 (2017).

169. Akdogan, Y., Emrullahoglu, M., Tatlidil, D., Ucuncu, M. & Cakan-Akdogan, G. EPR studies of intermolecular interactions and competitive binding of drugs in a drug–BSA binding model. *Physical Chemistry Chemical Physics* **18**, 22531–22539 (2016).

170. González-Sánchez, M. I., Lee, P. T., Guy, R. H. & Compton, R. G. In situ detection of salicylate in Ocimum basilicum plant leaves via reverse iontophoresis. *Chemical Communications* **51**, 16534–16536 (2015).

171. Chen, C. *et al.* Development of a structure-switching aptamer-based nanosensor for salicylic acid detection. *Biosens Bioelectron* **140**, 111342 (2019).

172. Wang, H. R. *et al.* Real time sensing of salicylic acid in infected tomato leaves using carbon tape electrodes modified with handed pencil trace. *Sens Actuators B Chem* **286**, 104–110 (2019).

173. Hu, Y. *et al.* In vivo detection of salicylic acid in sunflower seedlings under salt stress. *RSC Adv* **8**, 23404–23410 (2018).

174. Pham, J. *et al.* In vivo electrochemically-assisted polymerization of conjugated functionalized terthiophenes inside the vascular system of a plant. *Electrochem commun* **137**, 107270 (2022).

175. Cioć, M., Tokarz, K., Dziurka, M. & Pawłowska, B. Energy-saving led light affects the efficiency of the photosynthetic apparatus and carbohydrate content in gerbera jamesonii bolus ex hook. F. axillary shoots multiplied in vitro. *Biology (Basel)* **10**, 1035 (2021).

176. Pawłowska, B., Żupnik, M., Szewczyk-Taranek, B. & Cioć, M. Impact of LED light sources on morphogenesis and levels of photosynthetic pigments in Gerbera jamesonii grown in vitro. *Hortic Environ Biotechnol* **59**, 115–123 (2018).

177. Miao, Y., Chen, Q., Qu, M., Gao, L. & Hou, L. Blue light alleviates 'red light syndrome' by regulating chloroplast ultrastructure, photosynthetic traits and nutrient accumulation in cucumber plants. *Sci Hortic* **257**, 108680 (2019).

178. Sari, N., Antepli, E., Nartop, D. & Yetim, N. K. Polystyrene Attached Pt(IV)–Azomethine, Synthesis and Immobilization of Glucose Oxidase Enzyme. *Int J Mol Sci* **13**, 11870–11880 (2012).

179. Sungur, S. & Numanoğlu, Y. Development of Glucose Biosensor by Using Gelatin and Gelatin-Polyacrylamide Supporting Systems. *Artificial Cells, Blood Substitutes, and Biotechnology* **34**, 41–54 (2006).

180. Belyad, F., Karkhanei, A. A. & Raheb, J. Expression, characterization and one step purification of heterologous glucose oxidase gene from Aspergillus niger ATCC 9029 in Pichia pastoris. *EuPA Open Proteom* **19**, 1–5 (2018).

181. Rehman, M. *et al.* Light-emitting diodes: whether an efficient source of light for indoor plants? *Environ Sci Pollut Res* **24**, 24743–24752 (2017).

182. Seluzicki, A., Burko, Y. & Chory, J. Dancing in the dark: darkness as a signal in plants. *Plant Cell Environ* **40**, 2487–2501 (2017).

183. Poór, P. *et al.* Dark-induced changes in the activity and the expression of tomato hexokinase genes depend on the leaf age. *South African Journal of Botany* **118**, 98–104 (2018).

184. Scialdone, A. & Howard, M. How plants manage food reserves at night: quantitative models and open questions. *Front Plant Sci* **6**, 1–7 (2015).

185. Durgud, M. *et al.* Molecular Mechanisms Preventing Senescence in Response to Prolonged Darkness in a Desiccation-Tolerant Plant. *Plant Physiol* **177**, 1319–1338 (2018).

186. Asim, M. *et al.* Leaf senescence attributes: the novel and emerging role of sugars as signaling molecules and the overlap of sugars and hormones signaling nodes. *Crit Rev Biotechnol* 1–19 (2022) doi:10.1080/07388551.2022.2094215.

187. Luo, Y. *et al.* White-light emitting diodes' spectrum effect on photosynthesis and nutrient use efficiency in *Podocarpus macrophyllus* seedlings. *J Plant Nutr* **43**, 2876–2884 (2020).

188. Massa, G. *et al.* Light-emitting Diode Light Transmission through Leaf Tissue of Seven Different Crops. *HortScience* **50**, 501–506 (2015).

189. Meng, X. *et al.* LED-Supplied Red and Blue Light Alters the Growth, Antioxidant Status, and Photochemical Potential of in Vitro-Grown Gerbera jamesonii Plantlets. *Horticultural Science and Technology* **37**, 473–489 (2019).

190. Muneer, S., Kim, E., Park, J. & Lee, J. Influence of Green, Red and Blue Light Emitting Diodes on Multiprotein Complex Proteins and Photosynthetic Activity under Different Light Intensities in Lettuce Leaves (Lactuca sativa L.). *Int J Mol Sci* **15**, 4657–4670 (2014).

191. Johkan, M., Shoji, K., Goto, F., Hashida, S. nosuke & Yoshihara, T. Blue Light-emitting Diode Light Irradiation of Seedlings Improves Seedling Quality and Growth after Transplanting in Red Leaf Lettuce. *HortScience* **45**, 1809–1814 (2010).

192. Sami, F., Yusuf, M., Faizan, M., Faraz, A. & Hayat, S. Role of sugars under abiotic stress. *Plant Physiology and Biochemistry* **109**, 54–61 (2016).

193. Bita, C. E. & Gerats, T. Plant tolerance to high temperature in a changing environment: scientific fundamentals and production of heat stress-tolerant crops. *Front Plant Sci* **4**, 273 (2013).

194. Hasanuzzaman, M., Nahar, K., Alam, M. M., Roychowdhury, R. & Fujita, M. Physiological, Biochemical, and Molecular Mechanisms of Heat Stress Tolerance in Plants. *Int J Mol Sci* **14**, 9643–9684 (2013).

195. Martínez-Noël, G. M. A. & Tognetti, J. A. Sugar Signaling Under Abiotic Stress in Plants. in *Plant Metabolites and Regulation Under Environmental Stress* 397–406 (Academic Press, 2018). doi:10.1016/B978-0-12-812689-9.00022-4.

196. Aslam, M. *et al.* Plant Low-Temperature Stress: Signaling and Response. *Agronomy* **12**, 702 (2022).

197. Sharma, P. *et al.* The Role of Sugars in Improving Plant Abiotic Stress Tolerance. in *Improving Abiotic Stress Tolerance in Plants* 31–48 (CRC Press, 2020). doi:10.1201/9780429027505-3.

198. Gangola, M. P. & Ramadoss, B. R. Sugars Play a Critical Role in Abiotic Stress Tolerance in Plants. in *Biochemical, Physiological and Molecular Avenues for Combating Abiotic Stress Tolerance in Plants* 17–38 (Academic Press, 2018). doi:10.1016/B978-0-12-813066-7.00002-4.

199. Saha, S. R., Hossain, M. M., Rahman, M. M., Kuo, C. G. & Abdullah, S. Effect of high temperature stress on the performance of twelve sweet pepper genotypes. *Bangladesh J Agric Res* **35**, 525–534 (2010).

200. Li, F., Li, S. & Shan, Q. The Effect of Temperature on Plant Growth in Four Gerbera hybrida Cultivars. *HortScience* **54**, 1164–1167 (2019).

201. Dufault, R. J., Ward, B. & Hassell, R. L. Dynamic relationships between field temperatures and romaine lettuce yield and head quality. *Sci Hortic* **120**, 452–459 (2009).

202. Hara, M., Furukawa, J., Sato, A., Mizoguchi, T. & Miura, K. Abiotic Stress and Role of Salicylic Acid in Plants. *Abiotic Stress Responses in Plants* 235–251 (2012) doi:10.1007/978-1-4614-0634-1_13.

203. Prakash, V., Singh, V. P., Tripathi, D. K., Sharma, S. & Corpas, F. J. Nitric oxide (NO) and salicylic acid (SA): A framework for their relationship in plant development under abiotic stress. *Plant Biol* **23**, 39–49 (2021).

204. Zhao, P., Lu, G.-H. & Yang, Y.-H. Salicylic Acid Signaling and its Role in Responses to Stresses in Plants. *Mechanism of Plant Hormone Signaling under Stress* 413–441 (2017) doi:10.1002/9781118889022.CH17.

205. Santisree, P., Jalli, L. C. L., Bhatnagar-Mathur, P. & Sharma, K. K. Emerging Roles of Salicylic Acid and Jasmonates in Plant Abiotic Stress Responses. *Protective Chemical Agents in the Amelioration of Plant Abiotic Stress* 342–373 (2020) doi:10.1002/9781119552154.CH17.

206. Silber, A. *et al.* Irrigation of 'Hass' avocado: effects of constant vs. temporary water stress. *Irrig Sci* **37**, 451–460 (2019).

207. Chartzoulakis, K., Patakas, A., Kofidis, G., Bosabalidis, A. & Nastou, A. Water stress affects leaf anatomy, gas exchange, water relations and growth of two avocado cultivars. *Sci Hortic* **95**, 39–50 (2002).

208. Bonomelli, C., Celis, V., Lombardi, G. & Mártiz, J. Salt Stress Effects on Avocado (Persea americana Mill.) Plants with and without Seaweed Extract (Ascophyllum nodosum) Application. *Agronomy 2018, Vol. 8, Page 64* **8**, 64 (2018).

209. Bernstein, N., Meiri, A. & Zilberstaine, M. Root Growth of Avocado is More Sensitive to Salinity than Shoot Growth. *Journal of the American Society for Horticultural Science* **129**, 188–192 (2004).

210. Wang, C. F., Han, G. L., Yang, Z. R., Li, Y. X. & Wang, B. S. Plant Salinity Sensors: Current Understanding and Future Directions. *Front Plant Sci* **13**, (2022).

211. Tahamtan, A. & Ardebili, A. Real-time RT-PCR in COVID-19 detection: issues affecting the results. *Expert Rev Mol Diagn* **20**, 453–454 (2020).

212. Ruiz-Vega, G., Soler, M. & Lechuga, L. M. Nanophotonic biosensors for point-of-care COVID-19 diagnostics and coronavirus surveillance. *Journal of Physics: Photonics* **3**, 011002 (2021).

213. Zhang, Z. *et al.* Multiplex quantitative detection of SARS-CoV-2 specific IgG and IgM antibodies based on DNA-assisted nanopore sensing. *Biosens Bioelectron* **181**, 113134 (2021).

214. Chaibun, T. *et al.* Rapid electrochemical detection of coronavirus SARS-CoV-2. *Nat Commun* **12**, 802 (2021).

215. Kiew, L.-V. *et al.* Development of flexible electrochemical impedance spectroscopy-based biosensing platform for rapid screening of SARS-CoV-2 inhibitors. *Biosens Bioelectron* **183**, 113213 (2021).

216. Raziq, A. *et al.* Development of a portable MIP-based electrochemical sensor for detection of SARS-CoV-2 antigen. *Biosens Bioelectron* **178**, 113029 (2021).

217. Kim, S. *et al.* Vertical Flow Cellulose-Based Assays for SARS-CoV-2 Antibody Detection in Human Serum. *ACS Sens* **6**, 1891–1898 (2021).

218. Fabiani, L. *et al.* Magnetic beads combined with carbon black-based screen-printed electrodes for COVID-19: A reliable and miniaturized electrochemical immunosensor for SARS-CoV-2 detection in saliva. *Biosens Bioelectron* **171**, 112686 (2021).

219. Ezhilan, M., Suresh, I. & Nesakumar, N. SARS-CoV, MERS-CoV and SARS-CoV-2: A Diagnostic Challenge. *Measurement* **168**, 108335 (2021).

220. Yassine, A. Health Monitoring Systems for the Elderly During COVID-19 Pandemic: Measurement Requirements and Challenges. *IEEE Instrum Meas Mag* **24**, 6–12 (2021).

221. Diacci, C. *et al.* Diurnal in vivo xylem sap glucose and sucrose monitoring using implantable organic electrochemical transistor sensors. *iScience* **24**, 101966 (2021).

222. Wu, B. *et al.* Microelectrode glucose biosensor based on nanoporous platinum/graphene oxide nanostructure for rapid glucose detection of tomato and cucumber fruits. *Food Qual Saf* **6**, 1–11 (2022).

223. Giné Bordonaba, J. & Terry, L. A. Development of a Glucose Biosensor for Rapid Assessment of Strawberry Quality: Relationship between Biosensor Response and Fruit Composition. *J Agric Food Chem* **57**, 8220–8226 (2009).

224. Zheng, L. *et al.* A silk-microneedle patch to detect glucose in the interstitial fluid of skin or plant tissue. *Sens Actuators B Chem* **372**, 132626 (2022).

225. Diacci, C. *et al.* Real-Time Monitoring of Glucose Export from Isolated Chloroplasts Using an Organic Electrochemical Transistor. *Adv Mater Technol* **5**, 1900262 (2020).

226. Hossain, N. I. & Tabassum, S. A hybrid multifunctional physicochemical sensor suite for continuous monitoring of crop health. *Scientific Reports 2023 13:1* **13**, 1–18 (2023).